



Material microstructure optimization for linear elastodynamic energy wave management

Chau Le^a, Tyler E. Bruns^b, Daniel A. Tortorelli^{a,*}

^a University of Illinois at Urbana-Champaign, Champaign-Urbana, IL, USA

^b Champaign Simulation Center, Caterpillar Inc., Champaign, IL, USA

ARTICLE INFO

Article history:

Received 8 July 2010

Received in revised form

11 August 2011

Accepted 6 September 2011

Available online 22 September 2011

Keywords:

Energy wave management

Material design

Topology optimization

Sequentially ranked laminate

ABSTRACT

We describe a systematic approach to design material microstructures to achieve desired energy propagation in a two-phase composite plate. To generate a well-posed topology optimization problem we use the relaxation approach which requires homogenization theory to relate the macroscopic material properties to the microstructure, here a sequentially ranked laminate. We introduce an algorithm whereby the laminate layer volume fractions and orientations are optimized at each material point. To resolve numerical instabilities associated with the dynamic simulation and constrained optimization problem, we filter the laminate parameters. This also has the effect of generating smoothly varying microstructures which are easier to manufacture. To demonstrate our algorithm we design microstructure layouts for tailored energy propagation, i.e. energy focus, energy redirection, energy dispersion and energy spread.

© 2011 Elsevier Ltd. All rights reserved.

1. Introduction

The ability to manage energy propagation has received significant interest in the literature as it has applications in many fields such as impact/blast mitigation, crash worthiness, sound control, earthquake mitigation, etc. It has indeed been shown that acoustic waves can be redirected by utilizing material heterogeneity and anisotropy (Norris and Wickham, 2001; Amirkhizia et al., 2010). In this paper, we use topology optimization to systematically design material microstructures to achieve desired energy propagation. The material microstructure parameters are related to macroscopic material properties, i.e. elasticity tensor and mass density, via homogenization theory. Transient finite element analysis is employed to simulate the energy propagation in macroscopic structures and compute quantities of interests. Sensitivities of the interested quantities with respect to microstructure parameters are computed analytically via an adjoint method and used to iteratively update the design parameters by a gradient-based optimization algorithm. To demonstrate our algorithm, we optimize the material microstructure field of two-phase composite plates, cf. Fig. 1.

In topology optimization two or more material phases are optimally distributed to maximize structural performance, cf. Bendsøe and Sigmund (2003). Since we are designing anisotropic heterogeneous microstructures in an elastodynamics paradigm, topology optimization with relaxation via homogenization (Murat and Tartar, 1985; Kohn and Strang, 1986; Lurie and Cherkaev, 1986; Bendsøe and Kikuchi, 1988; Allaire, 2002; Cherkaev, 2000) is the obvious choice over topology optimization with restriction, e.g. via a solid isotropic material with penalization (SIMP) model (Bendsøe, 1989; Zhou and Rozvany, 1991). As such, the anisotropic heterogeneous microstructure is optimized at each material point to obtain the

* Corresponding author.

E-mail address: dtortore@illinois.edu (D.A. Tortorelli).

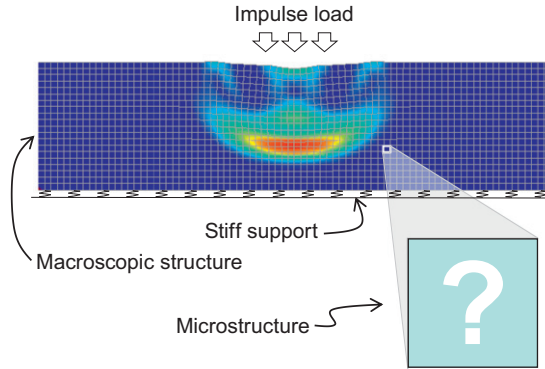


Fig. 1. Optimization problem overview. The contours indicate the total energy at a particular time instant.

most effective use of the constituent materials. This requires knowledge of the \mathcal{G} -closure, i.e. the set of achievable homogenized properties for the given phase volume fractions. Unfortunately, this \mathcal{G} -closure set of two isotropic phases is unknown in linear elasticity (refer to Bendsøe and Sigmund, 2003, p. 275 and bibliographical notes [4,5,25,34] for further discussion), although bounds on it are known, e.g. the Hashin and Shtrikman (1963) bounds. So instead, one assumes a specific microstructure and optimizes the parameters describing that microstructure, e.g. layer volume fractions and orientations in sequentially ranked laminates (Allaire, 2002; Allaire et al., 2004; Olhoff et al., 1998; Jacobsen et al., 1998; Díaz and Lipton, 1997), or the dimensions and orientation of a rectangular hole in a square cell (Bendsøe and Kikuchi, 1988; Rodrigues and Fernandes, 1995). Alternatively, one can employ a computationally intensive hierarchical approach using inverse homogenization to evaluate the optimal microstructure for the given volume fraction at each material point (Rodrigues et al., 1998, 2002). We use the former, i.e. specific microstructure approach wherein the laminate parameters are assigned and explicit formula (Allaire, 2002; Murat and Tartar, 1997) are used to obtain the homogenized material properties. Ultimately we optimize these laminate parameter fields to obtain the desired macroscopic response.

Dynamic response topology optimization based on frequency domain analysis, i.e. free vibration and forced response using Floquet–Bloch wave theory, has been widely researched to design both micro- and macrostructures. Refer to Bendsøe and Sigmund (2003) bibliographical note [14] for a comprehensive list of references. For example, inverse homogenization has been used to design phononic (elastic wave) (Sigmund and Jensen, 2003; Larsen et al., 2009) and photonic (Cox and Dobson, 2000; Nomura et al., 2009) unit cell microstructures. In other studies multiple materials are optimally distributed in a macroscopic domain to control wave propagation, e.g. Sigmund and Jensen (2003) for elastic, and Jensen and Sigmund (2005) and Frei et al. (2005) for electromagnetic applications. On the other hand, topology optimization for the more computationally intense dynamic structural response based on time domain analysis is less common, e.g. Min et al. (1999), Turteltaub (2005), and Dahl et al. (2008). Related is the optimization of damping distribution using Young measure relaxation in Munch et al. (2006). In this paper, the material microstructural field is optimized to generate the desired time-domain macroscopic energy propagation response.

Our work adopts the relaxation-homogenization topology optimization method (Cheng and Olhoff, 1982; Murat and Tartar, 1985; Kohn and Strang, 1986; Lurie and Cherkaev, 1986; Bendsøe and Kikuchi, 1988) to design the microstructure field for optimal macroscopic dynamic responses. At each material point, the laminate parameters for a sequentially ranked laminate are assigned and explicit homogenization formulae (Allaire, 2002; Murat and Tartar, 1997) are used to obtain the homogenized material properties. These homogenized properties, together with the trivially computed homogenized mass density, are used in an explicit finite element analysis to compute the structure's macroscopic dynamic response. An analytical sensitivity analysis follows to evaluate the cost and constraint function gradients with respect to the laminate parameters. Finally, an optimality criteria algorithm (refer to Bendsøe and Sigmund, 2003, pp. 9–10 and bibliographical note [7]) updates the laminate parameters, and the process is repeated until convergence is attained.

The remainder of the paper is organized as follows. Section 2 reviews homogenization theory and its application in topology optimization. The transient dynamic optimization problem is defined in Section 3, and the sensitivity analysis is detailed in Section 4. Numerical examples and conclusions are provided in Sections 5 and 6.

2. Homogenization

Most materials, such as steel, are not homogeneous on the microscopic scale, i.e. they contain heterogeneous microstructures. Nonetheless, since we are seldom interested in the microscopic behavior, and we treat these media as homogeneous with effective constitutive properties. Indeed, such effective properties are sufficient for computing most macroscopic responses of interest, e.g. energy and natural frequency.

Effective properties are often obtained by conducting experimental tests on representative samples. However, there are situations, e.g. in composite material design, where we know the constitutive properties of each constituent. In these

situations, we perform analytical or numerical “tests” to compute the effective properties. Much work has been devoted to this topic, cf. Hollister and Kikuchi (1992) for a review.

In a more specific case when the microstructure is periodic, only the unit cell needs to be analyzed to compute the effective properties. The derivation for this case is based on studies of partial differential equations with rapidly oscillating coefficients. We follow this homogenization approach under the assumption that the primary wave of interest has a wave length much longer than the unit cell size. Indeed, it is known that static homogenization theory holds in the usual sense, i.e. the displacement \mathbf{u}^e of the ε domain with elasticity tensor \mathbb{C}^e converges weakly to the displacement \mathbf{u} of the homogenized domain with elasticity tensor \mathbb{C}^h , when the unit cell size is infinitely small compared to propagating wave length (cf. Bensoussan et al., 1978). However, as discussed in Theorem 4.3 of Brahim-Otsmane et al. (1992), the energy of the $\mathbf{u}^e - \mathbb{C}^e$ response on the ε domain does not converge to that of $\mathbf{u} - \mathbb{C}^h$ response on the homogenized domain unless certain convergence restrictions are placed on the initial conditions. In this work we trivially satisfy these restrictions by assigning zero initial data. This subtle point is critical since we use energy in our cost function. If arbitrarily assigned, but smooth, initial data were assigned then the energy of the $\mathbf{u}^e - \mathbb{C}^e$ response on the ε domain exceeds that of $\mathbf{u} - \mathbb{C}^h$ response on the homogenized domain by a constant amount which depends on the microstructure. And while it is theoretically possible to compute this “corrector” (as well as its derivative for the optimization) it would be a computationally intractable task.

For a finite unit cell size, the homogenization process is an approximation of actual composite material. Characterization of this approximation is an interesting but challenging topic that is beyond the scope of this paper. Nonetheless, we provide a numerical study that gives a sense of how the homogenized response converges to the composite response as the unit cell size decreases.

Our numerical experiment consists of a rod fixed at the left end and subjected to a single sinusoidal pulse at the right end (cf. Fig. 2). The rod, of length 1024 mm, is made of a composite of alternating 50% stiff and 50% compliant materials where the stiff to compliant stiffness ratio of 66.67; the unit cell sizes are varied. The homogenized stiffness is 10^3 N/mm², the homogenized mass density is 1 g/mm, and the excitation frequency equals 190 Hz. We use the finite element method and discretize the rod into 1024 elements and the central difference time integration scheme with a uniform time step of 1/190 ms. This discretization is fine enough to resolve the local responses in the unit cells without using the homogenization approach. We then solve a homogeneous rod with an equivalent homogenized properties and compare the results. With this configuration, the response in the homogeneous rod is a perfect solitary wave whereas the responses in the composites deviate from the homogeneous one as the unit cell size increases. Notably, the homogenized response is completely different from the composite response when the number of unit cells per half wave length is $n=0.65$ (cf. Fig. 3a), and the two responses match well for $n \geq 5.2$ (cf. Fig. 3d). Of course this conclusion is applicable only for this particular problem, e.g., the results depend on the stiffness ratio, geometry of the unit cell, as well as macrogeometry.

Details of the homogenization theory can be found in e.g. Bensoussan et al. (1978) and Allaire (2002) wherein the elastodynamic governing equation

$$-\rho^e \ddot{\mathbf{u}}^e + \operatorname{div}(\mathbb{C}^e \hat{\nabla} \mathbf{u}^e) + \mathbf{b}^e = \mathbf{0} \quad \text{for } \mathbf{x} \in \Omega \quad (1)$$

with \mathbf{u}^e , ρ^e , \mathbb{C}^e , \mathbf{b}^e and \mathbf{x} the respective point-wise displacement, density, material elasticity tensor, body force and material point location, is replaced by the homogenized (averaged) equation

$$-\rho^h \ddot{\mathbf{u}} + \operatorname{div}(\mathbb{C}^h \hat{\nabla} \mathbf{u}) + \mathbf{b}^h = \mathbf{0} \quad \text{for } \mathbf{x} \in \Omega \quad (2)$$

with ρ^h , \mathbb{C}^h and \mathbf{b}^h the homogenized mass density, elasticity tensor and body force fields. Often and in this case, we are not interested in recovering the point-wise, i.e. local, responses in the microstructure, hence we only need to solve the homogenized equation for the averaged displacement field \mathbf{u} .

2.1. Sequentially ranked laminates

The sequentially ranked laminate, cf. Murat and Tartar (1997) and Allaire (2002), that we assume for our microstructure is constructed by laminating two materials: the reinforcement and matrix with elasticity tensors \mathbb{C}^+ and \mathbb{C}^- sequentially as follows. First, a rank-1 laminate is formed by layering the reinforcement with the matrix as depicted in Fig. 4. Two parameters describe this microstructure: the reinforcement layer volume fraction ρ_1 and the layer orientation φ_1 . Next, a rank-2 laminate is formed by layering the reinforcement with the rank-1 laminate using the analogous parameters ρ_2 and φ_2 . Similarly, a rank-3 laminate is formed by layering the reinforcement with the rank-1 laminate via the parameters ρ_3 and φ_3 . One continues this process to obtain rank- N laminates. We use rank-3 laminates for our two-dimensional design examples, since according to Lemma 2.39 in Allaire (2002), any two-(three-) dimensional



Fig. 2. Rod experiment configuration.

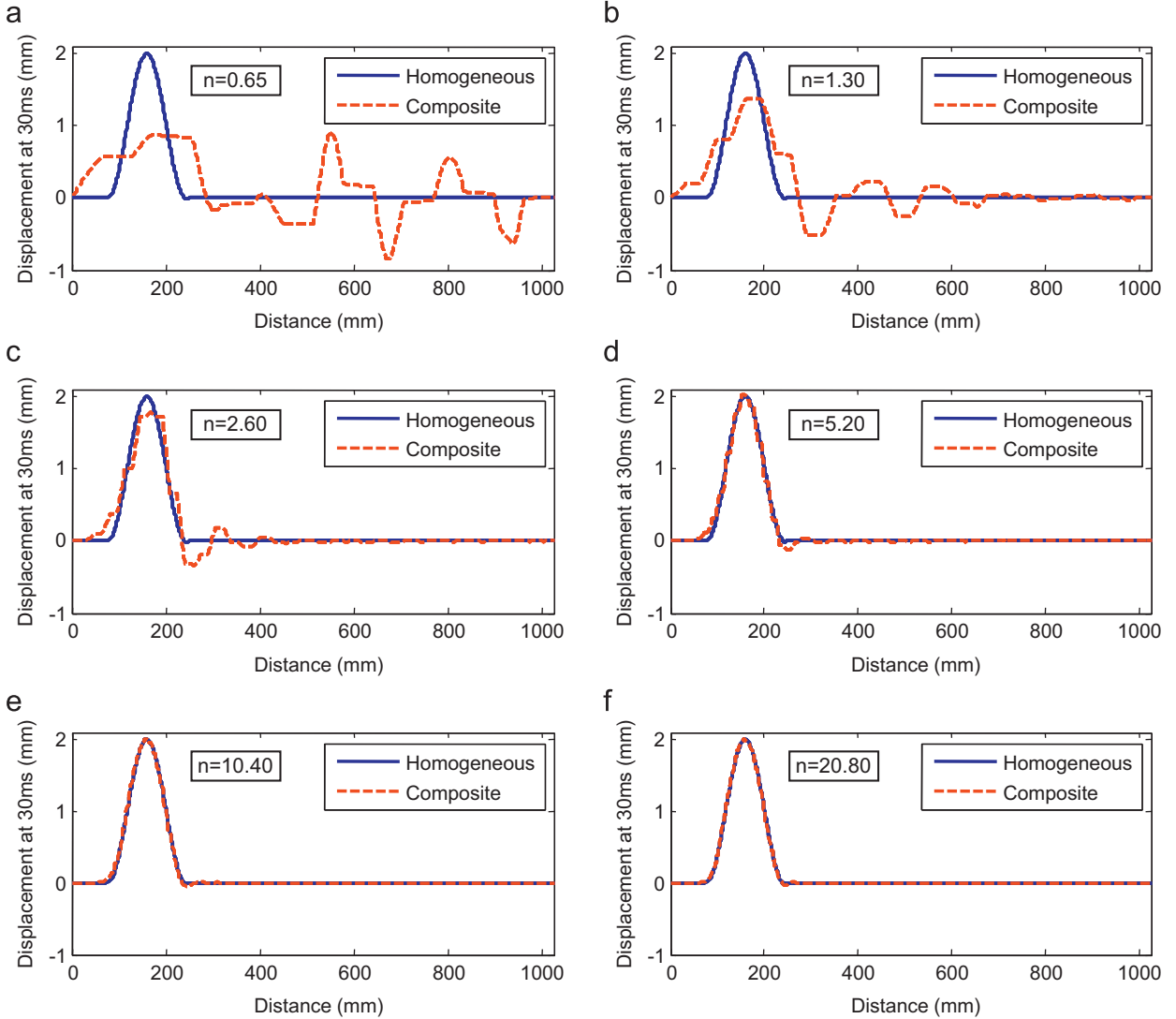


Fig. 3. Convergence of homogenized displacement as unit cell size decreases (n is the number of unit cells per half wave length).

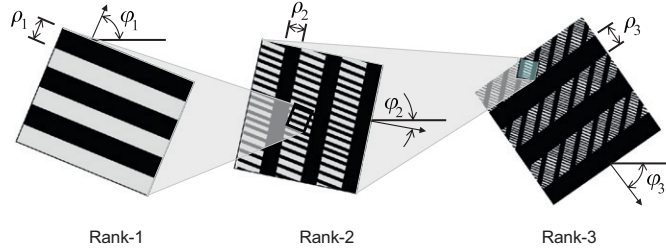


Fig. 4. Sequentially ranked laminates: the dark regions have stiffness C^+ whereas the gray regions have stiffness C^- .

elasticity tensor of an arbitrarily ranked laminate can be obtained by a rank-3(6) laminate. Note that in the above process, the intermediate product is always laminated with the same phase, namely C^+ . By interchanging the role of compliant and stiff materials in the above process, we obtain a second set of composites. Letting the role change arbitrary in each layer gives still another set of composites (which are not sequentially ranked laminate). The choice of the composite set does not appear to be critical in our subsequent optimization examples; indeed we show that rank-1 laminates can perform almost as well their higher rank counterparts. And of course for rank-1 laminates, these three sets of composites are identical.

The homogenized elasticity tensor \mathbb{C}^h for a sequentially ranked laminate can be derived analytically as follows. First, we obtain the formula for the rank-1 laminate by assuming an \mathbf{e}_1 lamination orientation and by solving the homogenization equations for the characteristic displacements. Then we evaluate the homogenized elasticity tensor components analytically. To accommodate a different lamination orientation \mathbf{e}_1^* , we simply apply the necessary rotation. Ultimately, we evaluate the rank-1 elasticity tensor \mathbb{C}^{h1} as

$$\mathbb{C}^{h1} = \mathbb{F}(\mathbb{C}^+, \mathbb{C}^-, \rho_1, \mathbf{e}_1^*) \quad (3)$$

To evaluate \mathbb{C}^{h2} , the rank-2 elasticity tensor, we substitute \mathbb{C}^+ , ρ_1 and \mathbf{e}_1^* with \mathbb{C}^{h1} , ρ_2 and \mathbf{e}_2^* and apply the above equation, i.e. $\mathbb{C}^{h2} = \mathbb{F}(\mathbb{C}^{h1}, \mathbb{C}^-, \rho_2, \mathbf{e}_2^*)$. To obtain the homogenized rank-N elasticity tensor, this recursive approach is repeated, and therefore it is amenable to computer implementation.

If the base materials are isotropic, with Lamé parameters μ^- and λ^- , a rather simple formula for the homogenized rank-N elasticity tensor \mathbb{C}^h is available, cf. Eq. (2.69) in Allaire (2002)

$$(1-\rho)(\mathbb{C}^h - \mathbb{C}^-)^{-1} = (\mathbb{C}^+ - \mathbb{C}^-)^{-1} + \rho \sum_{i=1}^N m_i \mathbb{F}^-(\mathbf{e}_i^*) \quad (4)$$

where ρ is the total volume fraction of the matrix material computed as

$$\rho = 1 - \prod_{i=1}^N (1-\rho_i) \quad (5)$$

and m_i are volume fraction like parameters satisfying

$$m_i = \frac{\rho_i}{\rho} \prod_{j=1}^{i-1} (1-\rho_j) \quad (6)$$

and

$$\sum_{i=1}^N m_i = 1 \quad \text{and} \quad m_i \geq 0 \quad (7)$$

$\mathbb{F}^-(\mathbf{e})$ is a fourth order tensor with major and minor symmetries defined by

$$\mathbb{F}^-(\mathbf{e}) = \frac{1}{\mu^-} (\mathbb{S}(\mathbf{e} \otimes \mathbf{e}) - (\mathbf{e} \otimes \mathbf{e}) \otimes (\mathbf{e} \otimes \mathbf{e})) + \frac{1}{2\mu^- + \lambda^-} (\mathbf{e} \otimes \mathbf{e}) \otimes (\mathbf{e} \otimes \mathbf{e}) \quad (8)$$

where \mathbb{S} is the fourth order symmetrizer.

To compute the sensitivity of \mathbb{C}^h we rewrite Eq. (4) as

$$\mathbb{C}^h = (1-\rho)\mathbb{D}^{-1} + \mathbb{C}^- \quad (9)$$

where

$$\mathbb{D} = (\mathbb{C}^+ - \mathbb{C}^-)^{-1} + \rho \sum_{i=1}^N m_i \mathbb{F}^-(\mathbf{e}_i^*) \quad (10)$$

so that the derivatives are

$$\frac{\partial \mathbb{C}^h}{\partial m_i} = -\rho(1-\rho)\mathbb{D}^{-1}\mathbb{F}(\mathbf{e}_i^*)\mathbb{D}^{-1} \quad (11)$$

$$\frac{\partial \mathbb{C}^h}{\partial \rho} = -\mathbb{D}^{-1} - (1-\rho)\mathbb{D}^{-1} \left[\sum_{i=1}^N m_i \mathbb{F}^-(\mathbf{e}_i^*) \right] \mathbb{D}^{-1} \quad (12)$$

$$\frac{\partial \mathbb{C}^h}{\partial \varphi_i} = -\rho(1-\rho)m_i \mathbb{D}^{-1} \frac{\partial \mathbb{F}(\mathbf{e}_i^*)}{\partial \varphi_i} \mathbb{D}^{-1} \quad (13)$$

where $\partial \mathbb{F}(\mathbf{e}_i^*) / \partial \varphi_i$ is obtained from Eq. (8) by noting that $\mathbf{e}_i^* = \{\mathbf{e}_1, \mathbf{e}_2\}^T = \{\cos \varphi, \sin \varphi\}^T$. Derivatives with respect to ρ_i are obtained by differentiating Eqs. (5) and (6), and applying the chain-rule to Eqs. (11) and (12).

2.2. Homogenization in the material layout problem

As mentioned earlier, we use topology optimization with the relaxation approach for our material microstructure design problem. This approach requires homogenization to define the elasticity tensor and the \mathcal{G} -closure to quantify the range of available homogenized elasticity tensors for given constituent materials and volume fractions. We do not know the \mathcal{G} closure, but we do know that the sequentially ranked laminate is optimal for some important design problems, e.g. compliance and natural frequency minimization (Allaire, 2002). For this reason, we use sequentially ranked laminates to

model our microstructure. Specifically, we use rank-3 laminates for our two-dimensional design problems, for as mentioned above, any two- (three-) dimensional elasticity tensor of an arbitrarily ranked laminate can be obtained by a rank-3(6) laminate. Thus we use six design parameters at each material point: three layer volume fractions ρ_1, ρ_2 and ρ_3 ; and three orientation angles φ_1, φ_2 and φ_3 . This is in contrast to other studies that use higher ranked laminates with fixed laminations, e.g. Allaire et al. (2004).

For verification purpose, we solve the following elastostatic finite element based design problem

$$\begin{aligned} \min_{\mathbf{d} \in \mathcal{A}} \quad & f(\mathbf{u}, \mathbb{C}^h) \\ \text{such that : } \quad & g_j(\mathbf{u}, \mathbb{C}^h) \leq 0, \quad j = 1, \dots, l \\ & \mathbf{K}(\mathbb{C}^h)\mathbf{u} = \mathbf{f} \\ & \mathbb{C}^h = \tilde{\mathbb{C}}^h(\mathbf{d}) \end{aligned} \quad (14)$$

for $A = \{0 \leq \rho_i \leq 1, \varphi_i \in \mathbb{R}\}$ where the design parameter vector \mathbf{d} is the collection of element laminate parameters $\rho_1, \rho_2, \rho_3, \varphi_1, \varphi_2$ and φ_3 ¹; f is the cost function; g_j are constraint functions; \mathbb{C}^h is the homogenized elasticity tensor; \mathbf{u} is the macroscopic finite element displacement vector; \mathbf{K} is the macroscopic finite element stiffness matrix; and \mathbf{f} is the macroscopic finite element force vector.

One generally uses mathematical programming methods such as the MMA (Svanberg, 1987) to solve this problem. However, we have either a single constraint, i.e. the explicit volume constraint in our static example, or no constraint (in our dynamic problem), so we use a simple, yet effective algorithm similar to the optimality criteria method (Bendsøe and Sigmund, 2003). Since the element laminate orientations φ_{ie} do not affect our constraint functions, their update is computed as

$$\begin{aligned} D_{ie} &= \frac{\partial f}{\partial \varphi_{ie}} \\ \varsigma &= -s_{ie}^\varphi \operatorname{sign}(D_{ie}) |D_{ie}|^\eta \\ \Delta \varphi_{ie} &= \max\{\nu^{\varphi-}, \min\{\nu^{\varphi+}, \varsigma\}\} \\ \varphi_{ie} &= \varphi_{ie} + \Delta \varphi_{ie} \end{aligned} \quad (15)$$

where η is a control parameter usually taken as 0.5; $\nu^{\varphi+}$ and $\nu^{\varphi-}$ are the upper and lower move limits; and s_{ie}^φ are positive scaling factors which are initially prescribed but updated at every optimization iteration based on whether the orientations φ_{ie} oscillate between successive iterations or not, cf. Svanberg (1987).

For problems with a total volume constraint, the element layer volume fractions ρ_{ie} are updated as

$$\begin{aligned} D_{ie} &= \frac{\partial f}{\partial \rho_{ie}} / \frac{\partial g}{\partial \rho_{ie}} - \Lambda \\ \varsigma &= -s_{ie}^\rho \operatorname{sign}(D_{ie}) |D_{ie}|^\eta \\ \Delta \rho_{ie} &= \max\{\nu^{\rho-}, \min\{\nu^{\rho+}, \varsigma\}\} \\ \rho_{ie} &= \rho_{ie} + \Delta \rho_{ie} \end{aligned} \quad (16)$$

where Λ is the Lagrange multiplier-like term computed, e.g. using the bi-section method, such that the updated design satisfies the volume constraint (Bendsøe and Sigmund, 2003). If no volume constraint is present, the ρ_{ie} are updated using Eq. (15).

As a static example, we design a transversely tip loaded cantilever beam for minimum compliance subject to a constraint that the isotropic reinforcement material can fill no more than 50% of the 2:1 rectangular design domain, cf. Fig. 5. Both materials have 0.3 Poisson's ratio and the stiff reinforcement material Young's modulus is 100 times greater than that of the compliant matrix material. We use quadratic 8-node quadrilateral (Q8) elements to prevent numerical instabilities that sometimes arise in such topology optimization problems due to Babuska–Brezzi like numerical instabilities (Diaz and Sigmund, 1995; Jog and Haber, 1996).

The optimized design appears in Fig. 5 where here and henceforth red represents the stiff-expensive reinforcement phase and blue the compliant-inexpensive matrix phase in the volume fraction plot. Although we use rank-3 microstructures, the optimized microstructures consist of rank-2 laminates with orthogonal members which agrees with theoretical studies (Allaire, 2002; Rozvany, 1998). We note that, because of degeneracies caused by the unnecessary third layer, the layer volume fraction and orientation fields of an individual layers are non-smooth in some regions. However, the corresponding microstructure field is smooth as seen in the blown-up of Fig. 5c. As expected, the bulk of the material is distributed to the beam's boundaries nearest the root. And away from these regions the microstructure forms a Michell truss like structure (Michell, 1904). Finally, to demonstrate the consistency of our computations, it is seen that two qualitatively equivalent designs are obtained from two different mesh discretizations, cf. Fig. 5a and h.

¹ We use anisotropic uniform material properties within each element.

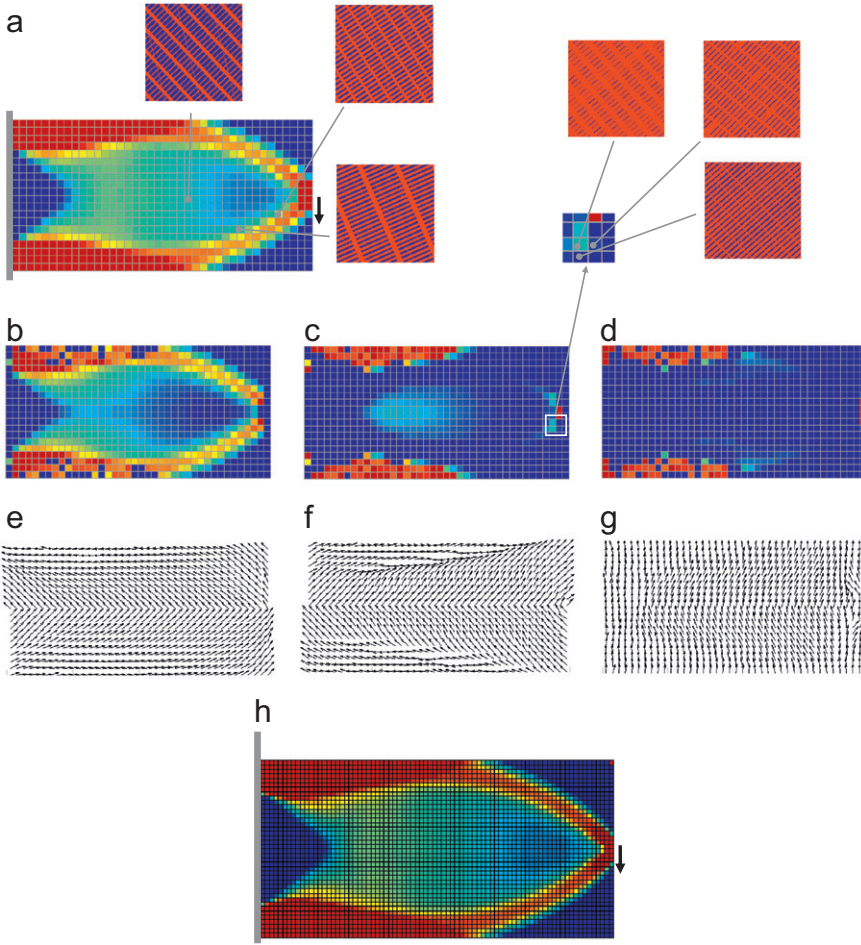


Fig. 5. Cantilever beam optimization for minimum compliance. (a) Optimal design (overall vol. frac.) obtained with 20x40 Q8 elements, (b) Vol. frac., layer 1, (c) Vol. frac., layer 2, (d) Vol. frac., layer 3, (e) Orientation, layer 1, (f) Orientation, layer 2, (g) Orientation, layer 3 and (h) Optimal design (overall vol. frac.) obtained with 40x80 Q8 elements. (For interpretation of the references to color in this figure legend, the reader is referred to the web version of this article.)

3. Transient optimization problem statement

Our dynamic simulations are intended to model energy propagating through solid bodies, hence we use an explicit finite element analysis. For simplicity and consistency, the optimization problem is stated in the discretized form as

$$\begin{aligned} \min_{\mathbf{d} \in \mathcal{A}} \quad & f(\mathbf{u}, \mathbb{C}^h, \rho^h) \\ \text{such that : } \quad & g_j(\mathbf{u}, \mathbb{C}^h, \rho^h) \leq 0, \quad j = 1, \dots, l \\ & \mathbf{M}(\rho^h) \ddot{\mathbf{u}} + \mathbf{K}(\mathbb{C}^h) \mathbf{u} = \mathbf{f} \\ & \mathbb{C}^h = \tilde{\mathbb{C}}^h(\mathbf{d}) \\ & \rho^h = \tilde{\rho}^h(\mathbf{d}) \end{aligned} \tag{17}$$

where \mathbf{M} is the macroscopic finite element mass matrix, and all other notation is the same as that described above.

Our design parameterization here is identical to that of the static problem, cf. Section 2.2. However, for our wave propagation analysis, we use bilinear 4-node quadrilateral (Q4) elements since Q8 elements are not suitable for explicit time integration (Cook et al., 2002). And unfortunately, Q4 elements are prone to Babuska–Brezzi like numerical instabilities in topology optimization (Diaz and Sigmund, 1995; Jog and Haber, 1996; Sigmund and Petersson, 1998). We resolve these instabilities by filtering each of the six element laminate parameter fields independently. This is in contrast to other methods that filter only the total volume fraction ρ (Allaire, 2002). Our filtering scheme also provides smoother variations of the microstructure fields which may ease manufacturing requirements.

In our examples, the objective functions involve the total energy in given elements e at time steps n which is given by

$$\mathcal{E}_e^{(n)} = \mathcal{U}_e^{(n)} + \mathcal{T}_e^{(n)} \quad (18)$$

where the element e strain energy at time step n , $\mathcal{U}_e^{(n)}$ is computed as

$$\mathcal{U}_e^{(n)} = \frac{1}{2} \mathbf{u}_e^{(n)T} \mathbf{K}_e \mathbf{u}_e^{(n)} \quad (19)$$

and the element e kinetic energy $\mathcal{T}_e^{(n)}$ is computed as

$$\mathcal{T}_e^{(n)} = \frac{1}{2} \dot{\mathbf{u}}_e^{(n)T} \mathbf{M}_e \dot{\mathbf{u}}_e^{(n)} \quad (20)$$

where \mathbf{K}_e and \mathbf{M}_e are the element e stiffness and mass matrices, respectively, $\mathbf{u}_e^{(n)}$ denotes the element e node displacement vector at time step n , and $\dot{\mathbf{u}}_e^{(n)}$ denotes the element e node velocity vector at time step n .

We also utilize the total input energy which is computed as

$$\mathcal{E}^{(in)} = \sum_{n=1}^N \mathbf{f}^{(n)T} \dot{\mathbf{u}}^{(n)} \Delta t \quad (21)$$

Our objective function often concerns the maximum total energy in a given space-time region. Since our gradient-based optimization algorithm requires smooth functions, we utilize the p -norm measure to approximate the maximum function as

$$\max_{e \in \Omega_s; n \in \mathcal{I}_t} (\mathcal{E}_e^{(n)}) \approx \mathcal{E}_{PN} = \left(\sum_{e \in \Omega_s} \left(\sum_{n \in \mathcal{I}_t} (\mathcal{E}_e^{(n)})^R \right)^{S/R} \right)^{1/S} \quad (22)$$

where Ω_s and \mathcal{I}_t are the sets of elements and time intervals corresponding to the given space-time region and $S=R=16$ unless otherwise noted.

4. Sensitivity analysis and optimization algorithm

We use gradient-based optimization algorithms which require the sensitivities of the objective and constraint functions with respect to design variables. The cost (and similarly constraint) function f is defined over the homogenized elasticity tensors \mathbb{C}^h , the homogenized mass densities ρ^h , and the displacement vectors $\mathbf{u}^{(n)}$ at every time step n . The displacement vectors $\mathbf{u}^{(n)}$ themselves are functions of \mathbb{C}^h and ρ^h which are in turn functions of the design parameter vector \mathbf{d} which contains the element laminate parameters, hence we write

$$f(\mathbf{d}) = \tilde{f}(\mathbf{u}^{(1)}(\mathbf{d}), \dots, \mathbf{u}^{(N)}(\mathbf{d}), \mathbf{d}) \quad (23)$$

where N is the total number of time steps.

We denote Df (without a subscript) as the total derivative of f with respect to its single argument \mathbf{d} , and $D_i \tilde{f}$ as the partial derivative of \tilde{f} with respect to argument i , e.g. $\mathbf{u}^{(i)}$. With this, the derivative Df is expressed as

$$Df = D_{N+1} \tilde{f} + \sum_{n=1}^N D\mathbf{u}^{(n)T} D_n \tilde{f} \quad (24)$$

The first term $D_{N+1} \tilde{f}$ is straightforward to compute since f is explicitly expressed in terms of \mathbf{d} . The second term, i.e. $\sum_{n=1}^N D\mathbf{u}^{(n)T} D_n \tilde{f}$, involves the displacement derivative $D\mathbf{u}^{(n)}$ which is implicitly defined via the governing equations. This is problematic.

To resolve the unknown displacement derivatives $D\mathbf{u}^{(n)}$ in Eq. (24) we use the adjoint method (Haug and Arora, 1978; Haug et al., 1986; Tortorelli et al., 1990; Michaleris et al., 1994). And to avoid numerical inconsistencies, we base our derivation on the fully, i.e. both spatially and temporally, discretized problem formulation.

$$\frac{1}{\Delta t^2} \mathbf{M} \mathbf{u}^{(n+1)} = \mathbf{f}^{(n)} + \left(\frac{2}{\Delta t^2} \mathbf{M} - \mathbf{K} \right) \mathbf{u}^{(n)} - \frac{1}{\Delta t^2} \mathbf{M} \mathbf{u}^{(n-1)} \quad (25)$$

where we use the energy conserving explicit central difference scheme (Hulbert and Chung, 1996) so that

$$\dot{\mathbf{u}}^{(n)} = \frac{1}{\Delta t^2} (\mathbf{u}^{(n+1)} - 2\mathbf{u}^{(n)} + \mathbf{u}^{(n-1)})$$

$$\dot{\mathbf{u}}^{(n)} = \frac{1}{2\Delta t} (\mathbf{u}^{(n+1)} - \mathbf{u}^{(n-1)}) \quad (26)$$

To initialize the time marching scheme, $\mathbf{u}^{(-1)}$ is computed from the initial displacement and velocity $\mathbf{u}^{(0)}$ and $\dot{\mathbf{u}}^{(0)}$ as

$$\mathbf{u}^{(-1)} = \frac{\Delta t^2}{2} \mathbf{M}^{-1} (\mathbf{f}^{(0)} - \mathbf{K} \mathbf{u}^{(0)}) + \mathbf{u}^{(0)} - \Delta t \dot{\mathbf{u}}^{(0)} \quad (27)$$

For the sensitivity analysis, we treat \mathbf{M} and \mathbf{K} as functions of \mathbf{d} , and differentiate the governing equation (25) with respect to \mathbf{d} to obtain

$$\frac{1}{\Delta t^2} D\mathbf{Mu}^{(n+1)} + \frac{1}{\Delta t^2} \mathbf{MDu}^{(n+1)} - D\mathbf{f}^{(n)} + \left(D\mathbf{K} - \frac{2}{\Delta t^2} D\mathbf{M} \right) \mathbf{u}^{(n)} + \left(\mathbf{K} - \frac{2}{\Delta t^2} \mathbf{M} \right) D\mathbf{u}^{(n)} + \frac{1}{\Delta t^2} D\mathbf{Mu}^{(n-1)} + \frac{1}{\Delta t^2} \mathbf{MDu}^{(n-1)} = 0 \quad (28)$$

Multiplying the above zero expression with an adjoint vector $\lambda^{(N-n+1)}$, summing over all time steps, and adding the zero result to the derivative Df in Eq. (24) gives

$$Df = D_{N+1}\tilde{f} + \sum_{n=1}^N D\mathbf{u}^{(n)\top} D_n\tilde{f} + \sum_{n=1}^N \lambda^{(N-n+1)} \left(\frac{1}{\Delta t^2} D\mathbf{Mu}^{(n)} + \frac{1}{\Delta t^2} \mathbf{MDu}^{(n)} - D\mathbf{f}^{(n-1)} + D\mathbf{Ku}^{(n-1)} + \mathbf{KDu}^{(n-1)} - \frac{2}{\Delta t^2} D\mathbf{Mu}^{(n-1)} \right. \\ \left. - \frac{2}{\Delta t^2} \mathbf{MDu}^{(n-1)} + \frac{1}{\Delta t^2} D\mathbf{Mu}^{(n-2)} + \frac{1}{\Delta t^2} \mathbf{MDu}^{(n-2)} \right) \quad (29)$$

Rearranging the above to isolate the implicitly defined displacement derivatives $D\mathbf{u}^{(n)}$ gives

$$Df = D_{N+1}\tilde{f} + \sum_{n=1}^N \lambda^{(N-n+1)\top} \left(\frac{1}{\Delta t^2} D\mathbf{Mu}^{(n)} - D\mathbf{f}^{(n-1)} + D\mathbf{Ku}^{(n-1)} - \frac{2}{\Delta t^2} D\mathbf{Mu}^{(n-1)} + \frac{1}{\Delta t^2} D\mathbf{Mu}^{(n-2)} \right) \\ + \sum_{n=1}^N \lambda^{(N-n+1)\top} \left(\frac{1}{\Delta t^2} \mathbf{MDu}^{(n)} + \mathbf{KDu}^{(n-1)} - \frac{2}{\Delta t^2} \mathbf{MDu}^{(n-1)} + \frac{1}{\Delta t^2} \mathbf{MDu}^{(n-2)} \right) + \sum_{n=1}^N (D\mathbf{u}^{(n)\top}) D_n\tilde{f} \quad (30)$$

and finally expanding the last two summations in Eq. (30) we obtain

$$Df = D_{N+1}\tilde{f} + \sum_{n=1}^N \lambda^{(N-n+1)\top} \left(\frac{1}{\Delta t^2} D\mathbf{Mu}^{(n)} - D\mathbf{f}^{(n-1)} + D\mathbf{Ku}^{(n-1)} - \frac{2}{\Delta t^2} D\mathbf{Mu}^{(n-1)} + \frac{1}{\Delta t^2} D\mathbf{Mu}^{(n-2)} \right) \\ + \lambda^{(N)\top} \mathbf{ODu}^{(1)} + \lambda^{(N-1)\top} \mathbf{ODu}^{(2)} + \dots + \lambda^{(4)\top} \mathbf{ODu}^{(N-3)} + \lambda^{(3)\top} \mathbf{ODu}^{(N-2)} + \lambda^{(2)\top} \mathbf{ODu}^{(N-1)} + \lambda^{(1)\top} \mathbf{ODu}^{(N)} \\ + \lambda^{(N)\top} \mathbf{PDu}^{(0)} + \lambda^{(N-1)\top} \mathbf{PDu}^{(1)} + \lambda^{(N-2)\top} \mathbf{PDu}^{(2)} + \dots + \lambda^{(3)\top} \mathbf{PDu}^{(N-3)} + \lambda^{(2)\top} \mathbf{PDu}^{(N-2)} + \lambda^{(1)\top} \mathbf{PDu}^{(N-1)} \\ + \lambda^{(N)\top} \mathbf{QDu}^{(-1)} + \lambda^{(N-1)\top} \mathbf{QDu}^{(0)} + \lambda^{(N-2)\top} \mathbf{QDu}^{(1)} + \lambda^{(N-3)\top} \mathbf{QDu}^{(2)} + \dots + \lambda^{(2)\top} \mathbf{QDu}^{(N-3)} + \lambda^{(1)\top} \mathbf{QDu}^{(N-2)} \\ + D_1\tilde{f} D\mathbf{u}^{(1)} + D_2\tilde{f} D\mathbf{u}^{(2)} + \dots + D_{N-3}\tilde{f} D\mathbf{u}^{(N-3)} + D_{N-2}\tilde{f} D\mathbf{u}^{(N-2)} + D_{N-1}\tilde{f} D\mathbf{u}^{(N-1)} + D_N\tilde{f} D\mathbf{u}^{(N)} \quad (31)$$

where $\mathbf{O} \equiv (1/\Delta t^2)\mathbf{M}$; $\mathbf{P} \equiv \mathbf{K} - (2/\Delta t^2)\mathbf{M}$; and $\mathbf{Q} \equiv (1/\Delta t^2)\mathbf{M}$.

We now define the adjoint problem such that its solution $\lambda^{(n)}$ annihilates the coefficients of the unknown derivatives $D\mathbf{u}^{(n)}$ (excluding $D\mathbf{u}^{(-1)}$ and $D\mathbf{u}^{(0)}$ since these derivatives are known functions of the initial conditions) in the above equation as follows:

$$\begin{aligned} \mathbf{O}\lambda^{(1)} + D_N\tilde{f} &= 0 \\ \mathbf{O}\lambda^{(2)} + \mathbf{P}\lambda^{(1)} + D_{N-1}\tilde{f} &= 0 \\ \mathbf{O}\lambda^{(3)} + \mathbf{P}\lambda^{(2)} + \mathbf{Q}\lambda^{(1)} + D_{N-2}\tilde{f} &= 0 \\ \mathbf{O}\lambda^{(n)} + \mathbf{P}\lambda^{(n-1)} + \mathbf{Q}\lambda^{(n-2)} + D_{N-3}\tilde{f} &= 0 \\ \dots &= 0 \\ \mathbf{O}\lambda^{(N)} + \mathbf{P}\lambda^{(N-1)} + \mathbf{Q}\lambda^{(N-2)} + D_1\tilde{f} &= 0 \end{aligned} \quad (32)$$

These equations are similar to the governing equations (cf. Eq. (25)). For example, substituting \mathbf{O} , \mathbf{P} and \mathbf{Q} for $n \geq 3$ gives

$$\frac{1}{\Delta t^2} \mathbf{M}\lambda^{(n+1)} = -D_{N-2}\tilde{f} + \left(\frac{2}{\Delta t^2} \mathbf{M} - \mathbf{K} \right) \lambda^{(n)} - \frac{1}{\Delta t^2} \mathbf{M}\lambda^{(n-1)} \quad (33)$$

The adjoint problem is an initial value problem thanks to the use of discrete convolution while deriving Eq. (29), i.e. Eq. (28) at time step n is multiplied with $\lambda^{(N-n+1)}$. If we instead multiplied Eq. (28) at time step n with $\lambda^{(n)}$ we would obtain a terminal value adjoint problem. In either case, we need to perform the primal analysis and store the vectors $\mathbf{u}^{(n)}$ before proceeding with the adjoint problem.

Upon solving the adjoint problem, the implicitly defined derivatives $D\mathbf{u}^{(n)}$ are annihilated and the sensitivity reduces to

$$Df = D_{N+1}\tilde{f} + \sum_{n=1}^N \lambda^{(N-n+1)\top} \left(\frac{1}{\Delta t^2} D\mathbf{Mu}^{(n)} - D\mathbf{f}^{(n-1)} + D\mathbf{Ku}^{(n-1)} - \frac{2}{\Delta t^2} D\mathbf{Mu}^{(n-1)} + \frac{1}{\Delta t^2} D\mathbf{Mu}^{(n-2)} \right) \\ + \lambda^{(N)\top} \mathbf{PDu}^{(0)} + \lambda^{(N-1)\top} \mathbf{QDu}^{(0)} + \lambda^{(N)\top} \mathbf{QDu}^{(-1)} \quad (34)$$

Fig. 6 shows the transient optimization flowchart. It starts with an initial design, i.e. the element laminate parameters, which are used to evaluate the homogenized properties. The primal analysis is performed, cf. Eq. (25), after which the adjoint analysis, cf. Eq. (32), and the sensitivity, cf. Eq. (34), are computed. This information is used by an optimizer to update the design, cf. Eqs. (15) and (16), and finally a convergence check is performed.

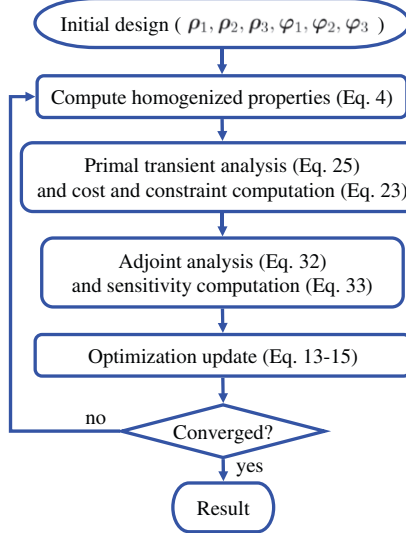


Fig. 6. Transient optimization flowchart.

Table 1
Material properties.

Material	Young's modulus (MPa)	Poison's ratio	Mass density (mg/mm ³)
Reinforcement	200,000 ^a	0.2	1.8
Matrix	3000 ^b	0.3	1.4

^a The reinforcement Young's modulus is in the range of carbon fiber.

^b The matrix Young's modulus is in the range of epoxy resin.

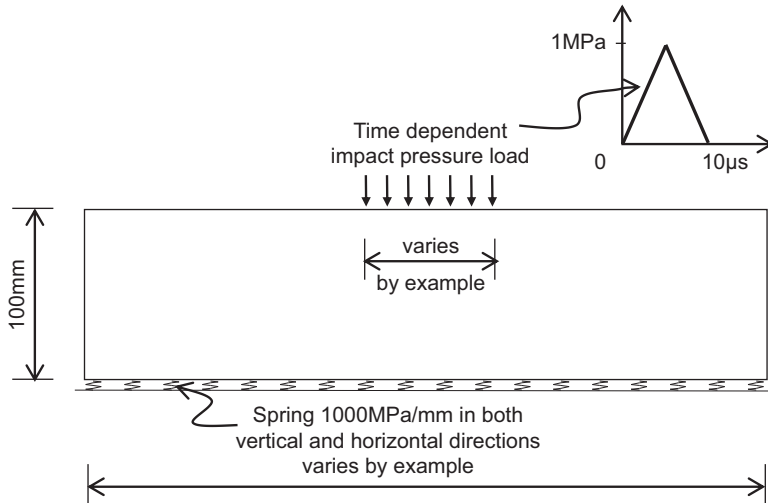


Fig. 7. Design problem description.

5. Numerical results

In the following examples, we optimize the microstructures of a 100 mm thick plate that is subjected to impact loading so that the input energy either propagates to or away from a given region. The plane strain plate is supported by linear elastic springs on the bottom, i.e. representing a stiff support. Properties of the constituent materials are denoted in Table 1. A uniform pressure load is applied over the loading region, cf. Fig. 7; it varies in a triangular fashion over the 10 μ s

loading interval. For simplicity the peak load is assumed to be 1 MPa, however changes in load magnitude do not change the design since we assume linear behavior. The duration of the transient simulation, which is typically 50 μ s, is chosen to allow the wave to reach the region of interest. For stability reasons, we use a constant time step interval with length $dt = 0.25 \mu$ s for all of the coarse mesh examples. In our mesh refinement studies the time step is decreased by the same factor as the element so as to satisfy the Courant–Fredericks–Lewy stability condition.

For each example, we describe the microstructure field by layer volume fraction contours and orientation vector fields. The orientation vectors indicate the direction of the material “fibers”. We also include plots of the total energy at various times to illustrate the energy wave propagation.

5.1. Energy focusing

In the first example, the 266.67 mm wide domain is subjected to an impact load distributed over the entire top surface, cf. Fig. 8. We desire to focus the energy to the center of the bottom surface. To achieve this, we maximize over time the sum of total energy in the 6.67 mm \times 16.67 mm rectangular region located at the plate's bottom center, and we use Eq. (22) with $S=1$ and $R=16$ for this objective function. The symmetric half domain is discretized using 30×40 Q4 elements.

For this configuration, a homogeneous plate would generate an almost plane wave without energy concentration. Whereas, as seen in Fig. 8, the optimized design effectively concentrates the energy to the desired region. We attribute this directionality to the presence of a compliant top region which accepts the load and a “funnel” of the predominantly stiff phase which directs the energy towards the desired region. Finally note that the microstructure field of this design (and all other designs in this section) has smoothly varying phase layer volume fractions and orientations. Such smoothness is attributed to the laminate parameter filter.

To demonstrate the convergence of our algorithm, we solve again this energy focusing problem with a finer mesh using 60×80 Q4 elements for the half domain while keeping the same filter radius. As shown in Fig. 9, the design generated with the refined mesh is qualitatively similar to the design with coarse mesh shown in Fig. 8.

To study the effect of the rank number on the ability of the structure to achieve the desired wave propagation, we repeat the problem using rank-1 and rank-2 laminates, cf. Figs. 10 and 11, where it is seen that the energy is effectively manipulated using lower rank laminates. This implies that effective wave tailoring may be maintained while imposing simpler microstructures which may be easier to manufacture.

In these examples it is also possible to discern how the layer orientations affect the design. Indeed, from the rank-1 design of Fig. 8 we see how the microstructure itself creates a funneling path for the energy transfer. Although less transparent, this same effect can be seen in the rank-2 and rank-3 designs of Figs. 8 and 11. Bear in mind the orientation of each phase loses its importance if its associated layer volume fraction is predominantly 0 or 1, i.e. blue or red, in which case the layer is nearly isotropic, cf. the top right microstructure inset in Fig. 21.

5.2. Energy redirecting

In this example, a 600 mm \times 100 mm symmetric domain is subjected to an impact load over the 100 mm wide top center surface. The goal is to redirect the input energy to various regions in the design domain: (1) a 15 mm \times 5 mm region centered 42.5 mm left of the bottom right corner; (2) a 5 mm \times 5 mm region centered 42.5 mm above the bottom right corner; (3) a 5 mm \times 10 mm region centered 150 mm left of the top right corner; and (4) a 5 mm \times 5 mm region centered 47.5 mm above and 102.5 mm left of the bottom right corner. To achieve these goals, the objective functions are formulated to maximize the normalized total energy over the target regions which is one finite element in size in this case, i.e.

$$f = \frac{\mathcal{E}_{PN}}{\mathcal{E}^{(in)}} \quad (35)$$

where \mathcal{E}_{PN} and $\mathcal{E}^{(in)}$ are given in Eqs. (21) and (22). Using symmetry, we model half of the domain with 20×60 Q4 elements.

Fig. 12 shows the wave propagation through a homogeneous plate composed of (a) the matrix material and (b) the reinforcement material. Figs. 13–16 show the optimized microstructures as well as energy wave propagation for the four objectives. In all cases it can be seen that the energy is effectively channeled to the desired regions. Upon comparing Figs. 8 and 13, we again see that the optimized design consists of a compliant top region which accepts the load and the funnel of the predominantly stiff phase which directs the energy towards the desired region. Whereas in Fig. 14 the load region is stiff, possibly to limit the amount of “vertically traveling” energy into the domain. But like the other designs, a funnel of the predominantly stiff phase directs the energy towards the desired region. Like the designs of Figs. 8 and 13, the design of Fig. 15 consists of a compliant top region to accept the energy, as well as a funnel of the predominantly stiff phase to direct the energy towards the desired region. Note here however, the appearance of the largish stiff phase region just below the load surface; its presence limits energy travel towards plate's bottom. Similar comments can be made regarding the design of Fig. 16.

5.3. Energy dispersing

This example is identical to the previous example except that the objective here is to prevent the energy from propagating to the bottom 5 mm wide region of the plate. Two objective functions are utilized: (1) minimizing the

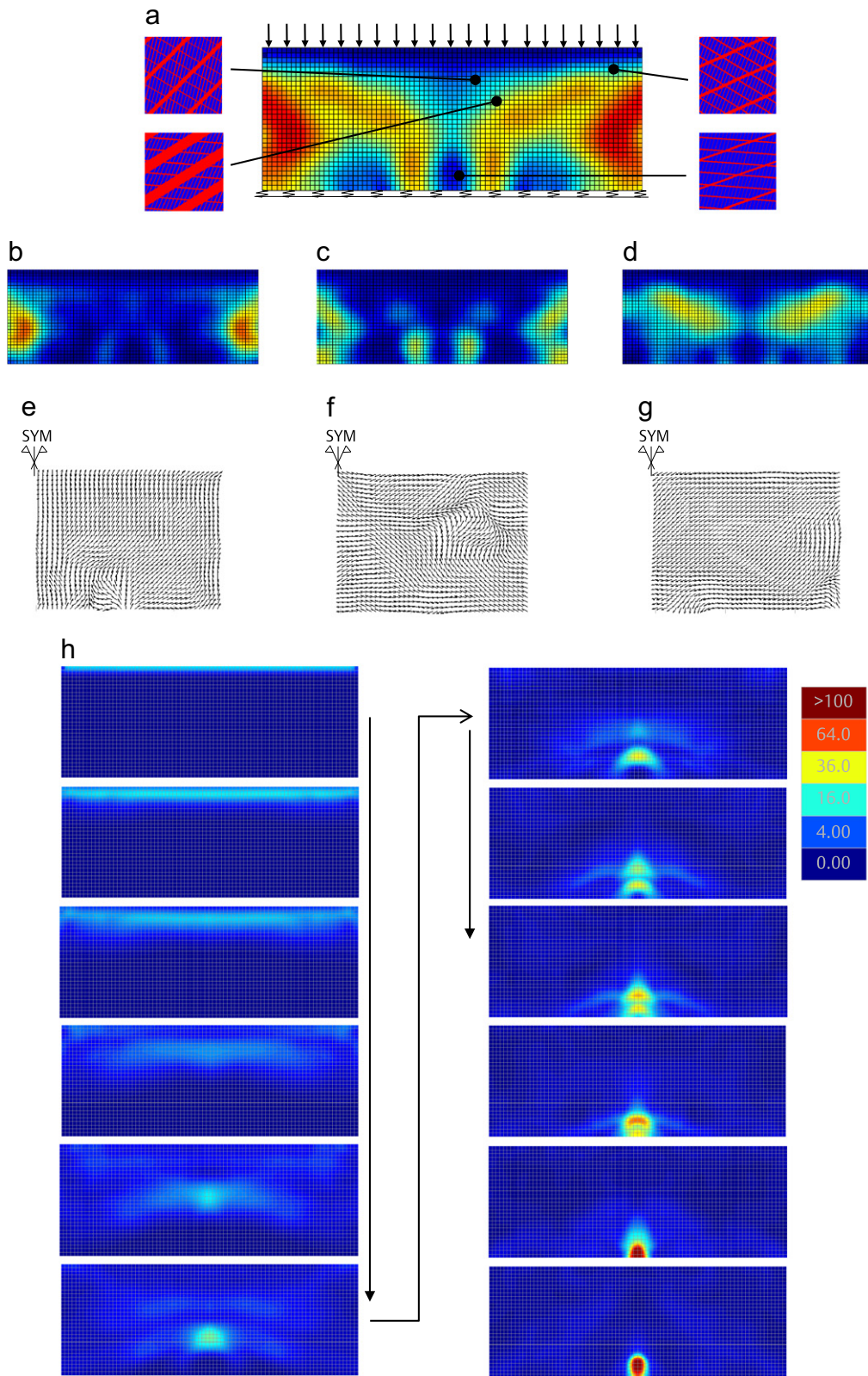


Fig. 8. Energy focusing design: find the rank-3 laminate microstructure to concentrate energy to middle bottom spot. (a) Optimal design (overall vol. frac.), (b) Vol. frac., layer 1, (c) Vol. frac., layer 2, (d) Vol. frac., layer 3, (e) Orientation, layer 1, (f) Orientation, layer 2, (g) Orientation, layer 3 and (h) Total energy at times 3.75, 8.25, 10.0, 12.5, 16.25, 20.0, 23.75, 27.5, 30.0, 32.5, 40.0 and 48.8 μ s. (For interpretation of the references to color in this figure legend, the reader is referred to the web version of this article.)

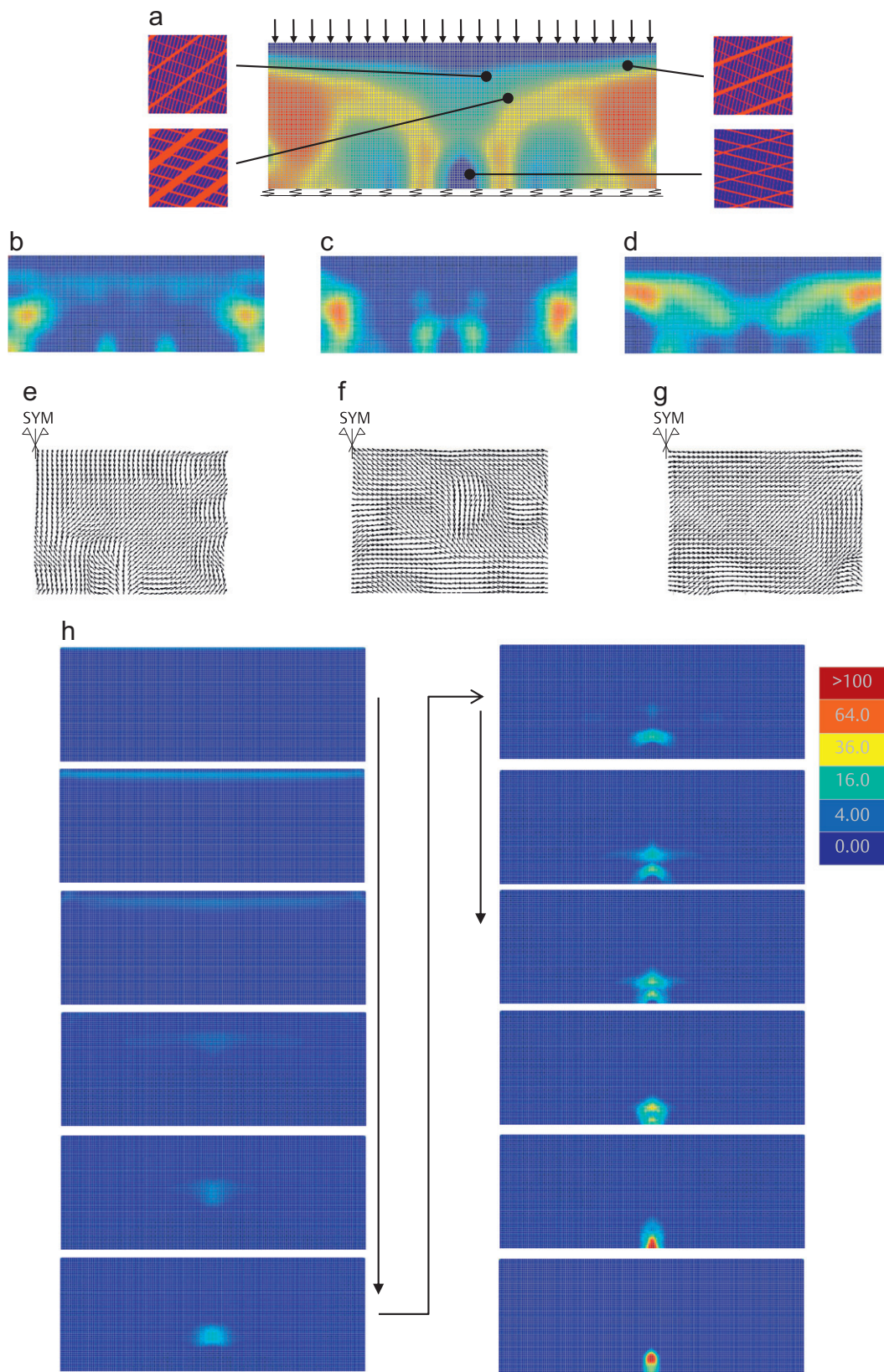


Fig. 9. Energy focusing design: repeat example in Fig. 8 with a refined mesh. (a) Optimal design (overall vol. frac.), (b) Vol. frac., layer 1, (c) Vol. frac., layer 2, (d) Vol. frac., layer 3, (e) Orientation, layer 1, (f) Orientation, layer 2, (g) Orientation, layer 3 and (h) Total energy at times 3.75, 8.25, 10.0, 12.5, 16.25, 20.0, 23.75, 27.5, 30.0, 32.5, 40.0 and 48.8 μ s.

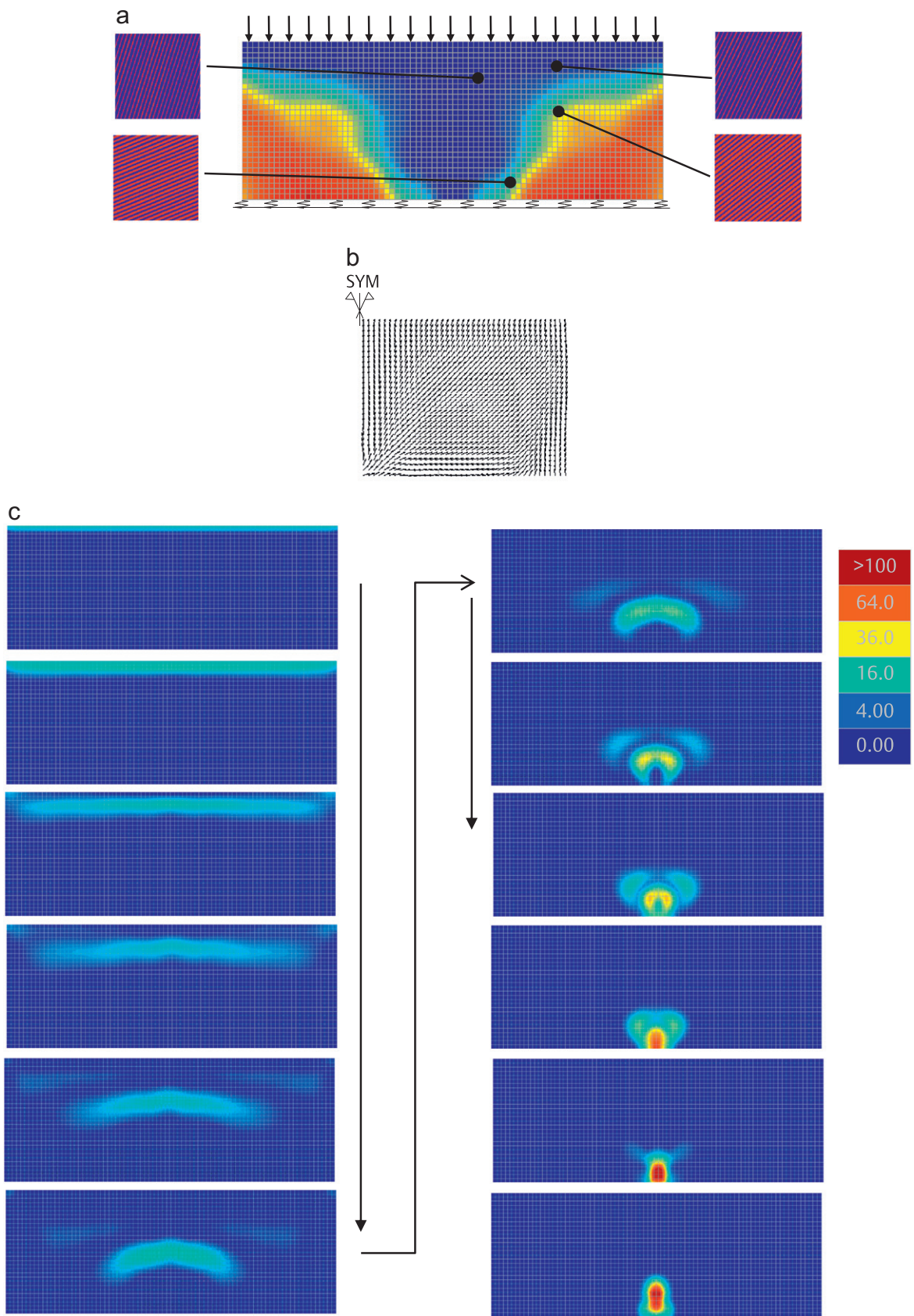


Fig. 10. Energy focusing design: repeat example in Fig. 8 using rank-1 laminate. (a) Optimal design (overall vol. frac.), (b) Orientation, layer 1 and (c) Total energy at times 3.75, 8.25, 10.0, 12.5, 16.25, 20.0, 23.75, 27.5, 30.0, 32.5, 40.0 and 48.8 μ s.

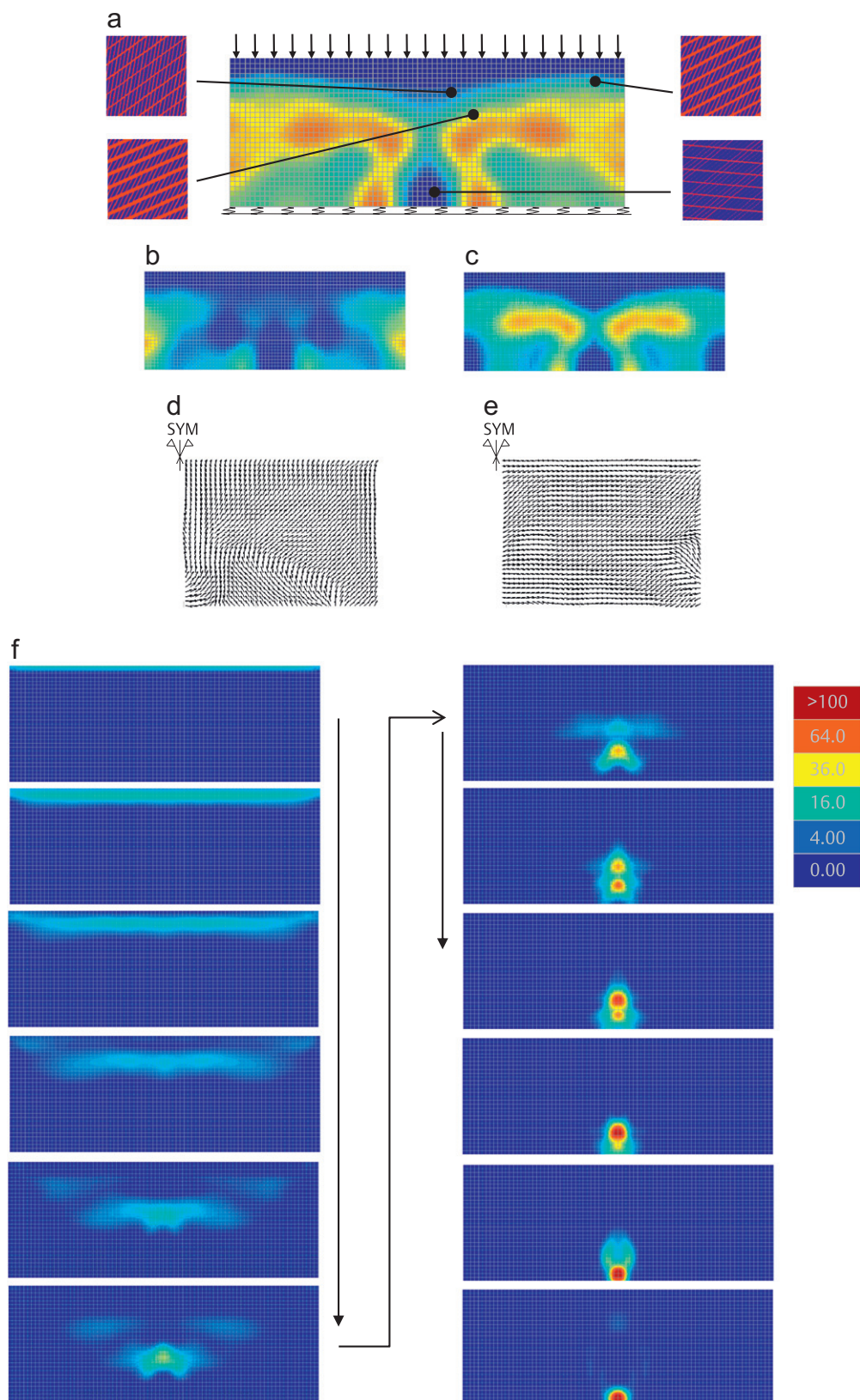


Fig. 11. Energy focusing design: repeat example in Fig. 8 using rank-2 laminate. (a) Optimal design (overall vol. frac.), (b) Vol. frac., layer 1, (c) Vol. frac., layer 2, (d) Orientation, layer 1, (e) Orientation, layer 2 and (f) Total energy at times 3.75, 8.25, 10.0, 12.5, 16.25, 20.0, 23.75, 27.5, 30.0, 32.5, 40.0 and 48.8 μ s. (For interpretation of the references to color in this figure legend, the reader is referred to the web version of this article.)

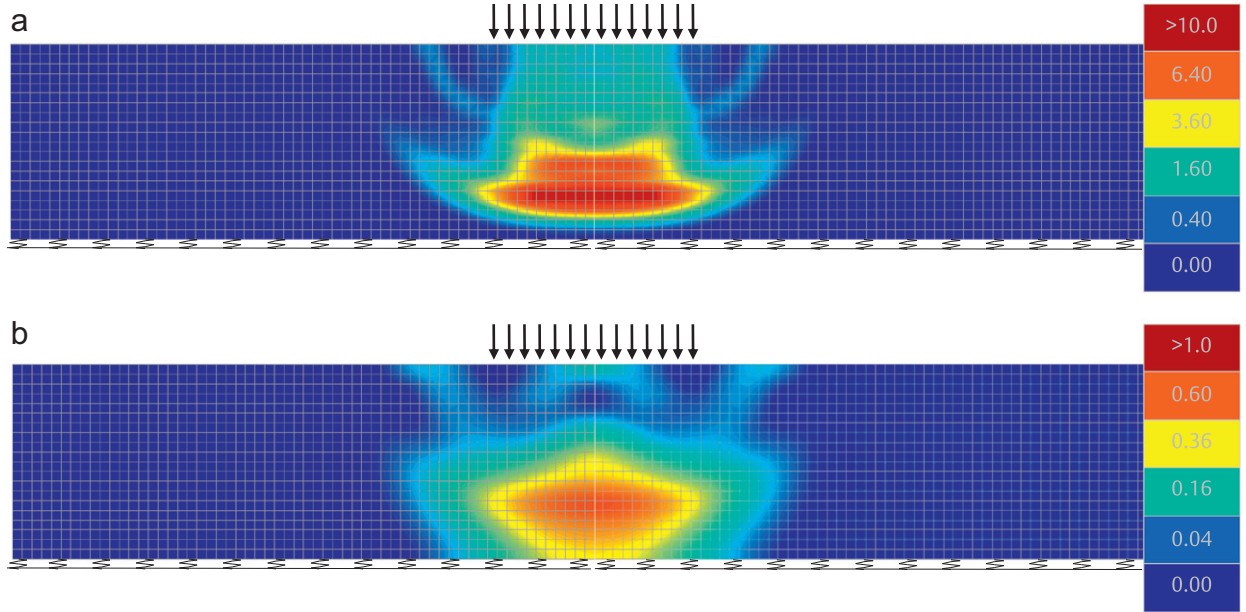


Fig. 12. Wave propagation through a pure matrix (a) and reinforcement (b) plate. (a) Pure matrix material: total energy density at time step 52.5 μs and (b) Pure reinforcement material: total energy density at time step 11.2 μs .

maximum total energy at bottom of the plate, cf. Eq. (22); and (2) minimizing the same maximum total energy normalized by the total input energy, cf. Eq. (35). The optimized microstructure field and the energy propagation corresponding to these two objective functions appear in Figs. 17 and 18, respectively. In the first case, we notice that stiff microstructures are assigned to the top and bottom regions. This makes sense because the stiff layer at the top lowers the input energy by reducing the displacement in the loading region while the stiff layer at the bottom helps reflect energy away from that region. In the second case, since the objective function is normalized by the input energy, the stiff layer only appears in the bottom region. In both cases, the energy appears to get trapped in local regions near the top surface.

Again, to study the effect of the rank number on the ability of the structure to achieve the desired wave propagation, we repeat the aforementioned second case, minimizing the maximum total energy over the bottom 600 mm \times 5 mm wide region normalized by the total input energy, using rank-1 and rank-2 laminates, cf. Figs. 19 and 20, where it is seen that the energy is effectively manipulated using lower rank laminates. Again, this implies that effective wave tailoring may be maintained while imposing simpler microstructures which may be easier to manufacture.

5.4. Energy spreading

In this example, the 160 mm wide domain is discretized using 80×50 Q4 elements, and the impact load is distributed over a 10 mm width on the top surface, cf. Fig. 21. In contrast to the first example, we desire to spread the energy evenly near the bottom surface. To achieve this, we match the element energy in the layer 20 mm above the bottom surface at time 16.7 μs to a specific 0.15 N mm value, by minimizing an RMS error function. The results are qualitatively insensitive to the choice of these specific time and energy values as long as they are in a reasonable range, e.g. we cannot have the wave traveling faster than that in a plate composed of pure stiff material and we cannot request more energy than that which is input to the plate. Reducing the time tends to produce an overall stiffer design that increases the wave speed, and increasing the energy value tends to produce a softer, i.e. more energy absorbing, design in the loading region. Figs. 21 and 22 show the results using rank-3 and rank-1 laminates, respectively. In both cases, the optimized designs generate almost uniform energy distributions in the desired space-time region. Here we again see the compliant top load region which accepts the energy; however the funnel of the predominantly stiff phase is lacking. Instead we see how the layer orientations, of phases 1 and 2 in particular, serve to channel the energy to the plate's extremities, cf. Fig. 21. This effect is even more transparent in the rank-1 design of Fig. 22.

5.5. Optimization robustness and analysis accuracy

Robustness refers to two separate issues: (1) the design's susceptibility to failure with respect to small fluctuations in loading, support, or geometric, etc. parameters; and (2) the dependence of the design on the finite element discretization. The first issue is addressed in reliability based topology optimization where probability density functions of such parameters are used rather than deterministic values and probabilities of failure serve as the objective and constraint

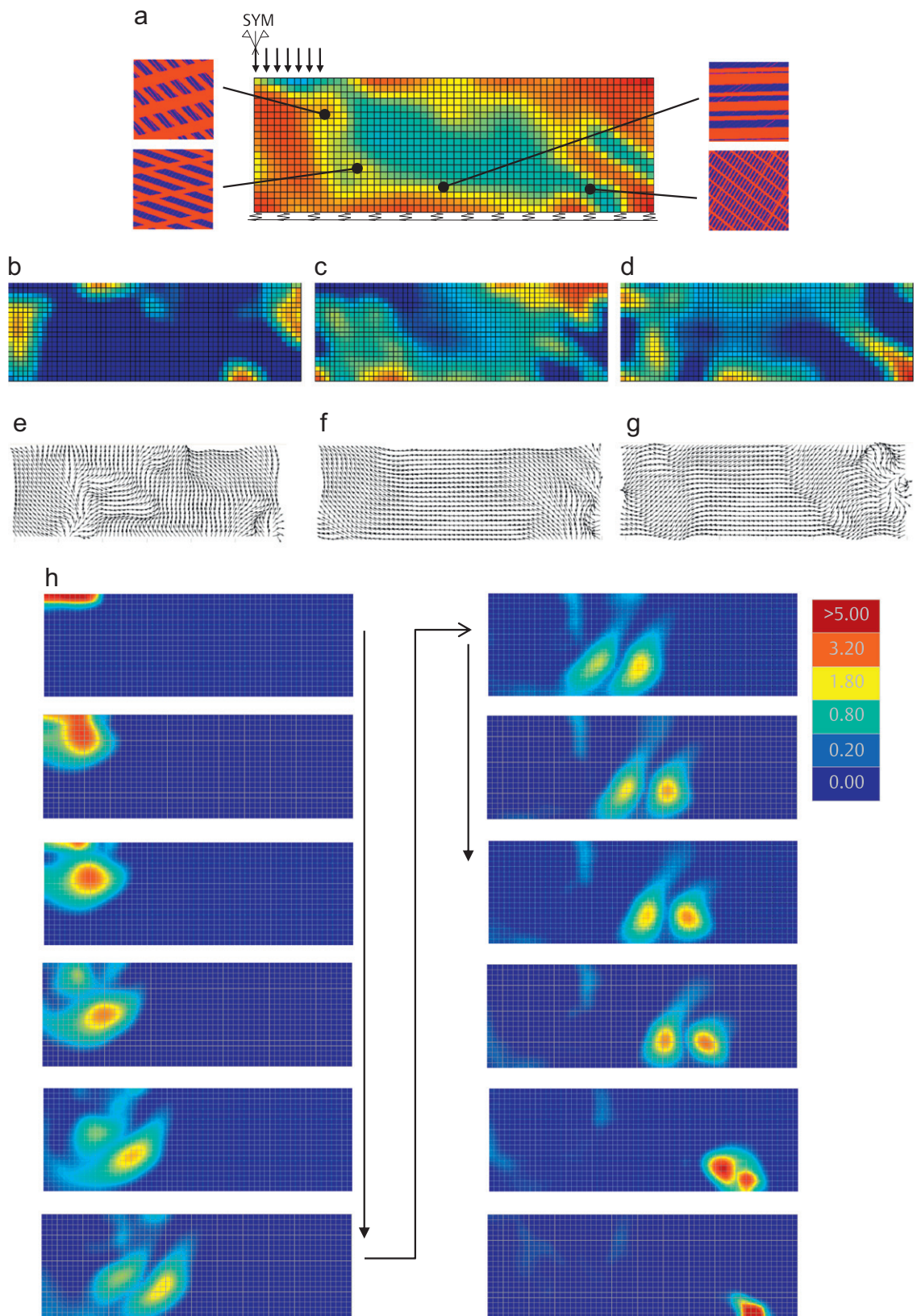


Fig. 13. Energy focusing design: find the rank-3 laminate microstructure to concentrate energy to a bottom region far from the center. (a) Optimal design (overall vol. frac.), (b) Vol. frac., layer 1, (c) Vol. frac., layer 2, (d) Vol. frac., layer 3, (e) Orientation, layer 1, (f) Orientation, layer 2, (g) Orientation, layer 3 and (h) Total energy at times 3.75, 7.5, 10.0, 12.5, 16.25, 20.0, 23.75, 27.5, 30.0, 32.5, 40.0 and 47.5 μ s.

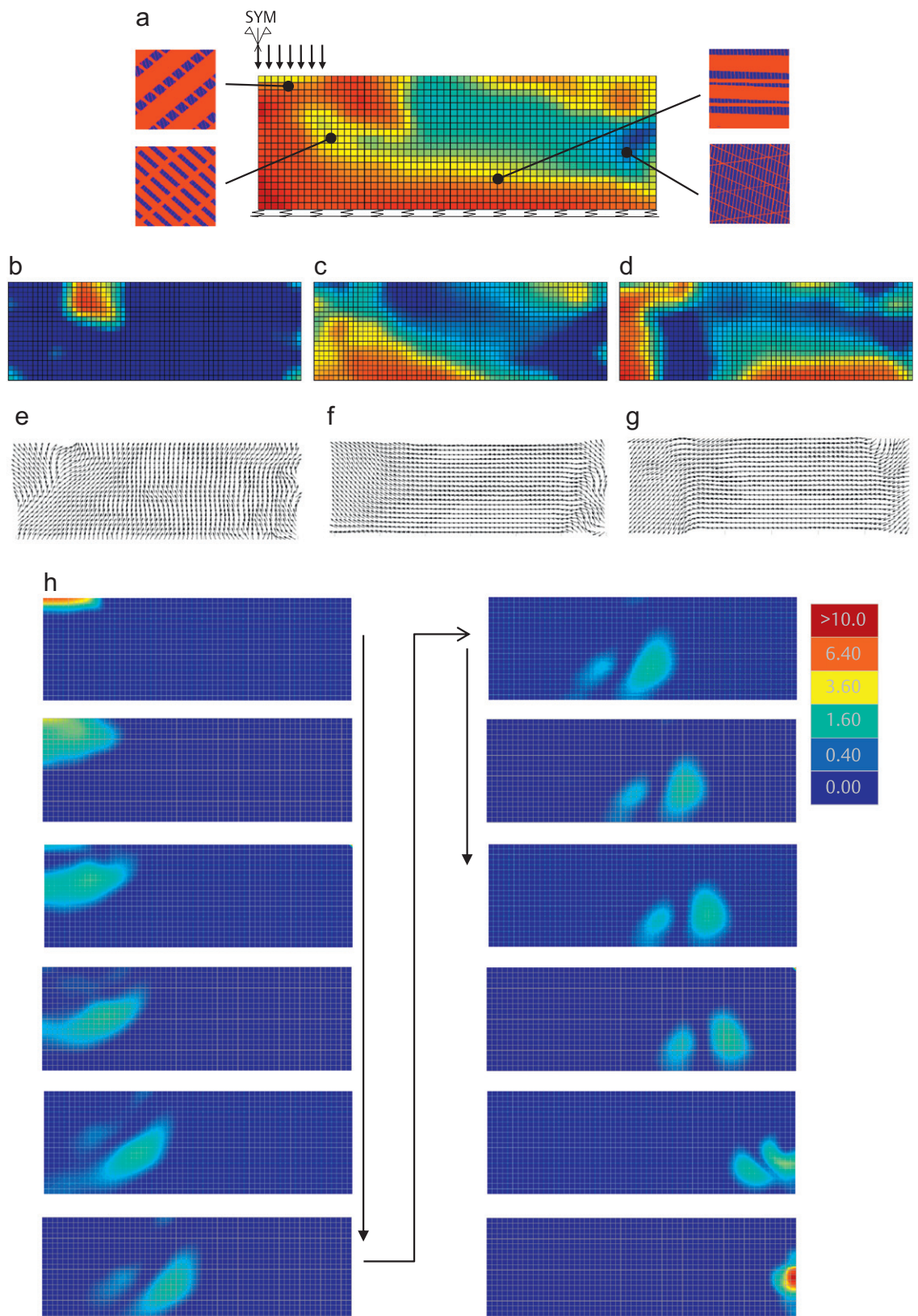


Fig. 14. Energy focusing design: find the rank-3 laminate microstructure to concentrate energy to a side region. (a) Optimal design (overall vol. frac.), (b) Vol. frac., layer 1, (c) Vol. frac., layer 2, (d) Vol. frac., layer 3, (e) Orientation, layer 1, (f) Orientation, layer 2, (g) Orientation, layer 3 and (h) Total energy at times 3.75, 7.5, 10.0, 12.5, 16.25, 20.0, 23.75, 27.5, 30.0, 32.5, 40.0 and 47.5 μ s.

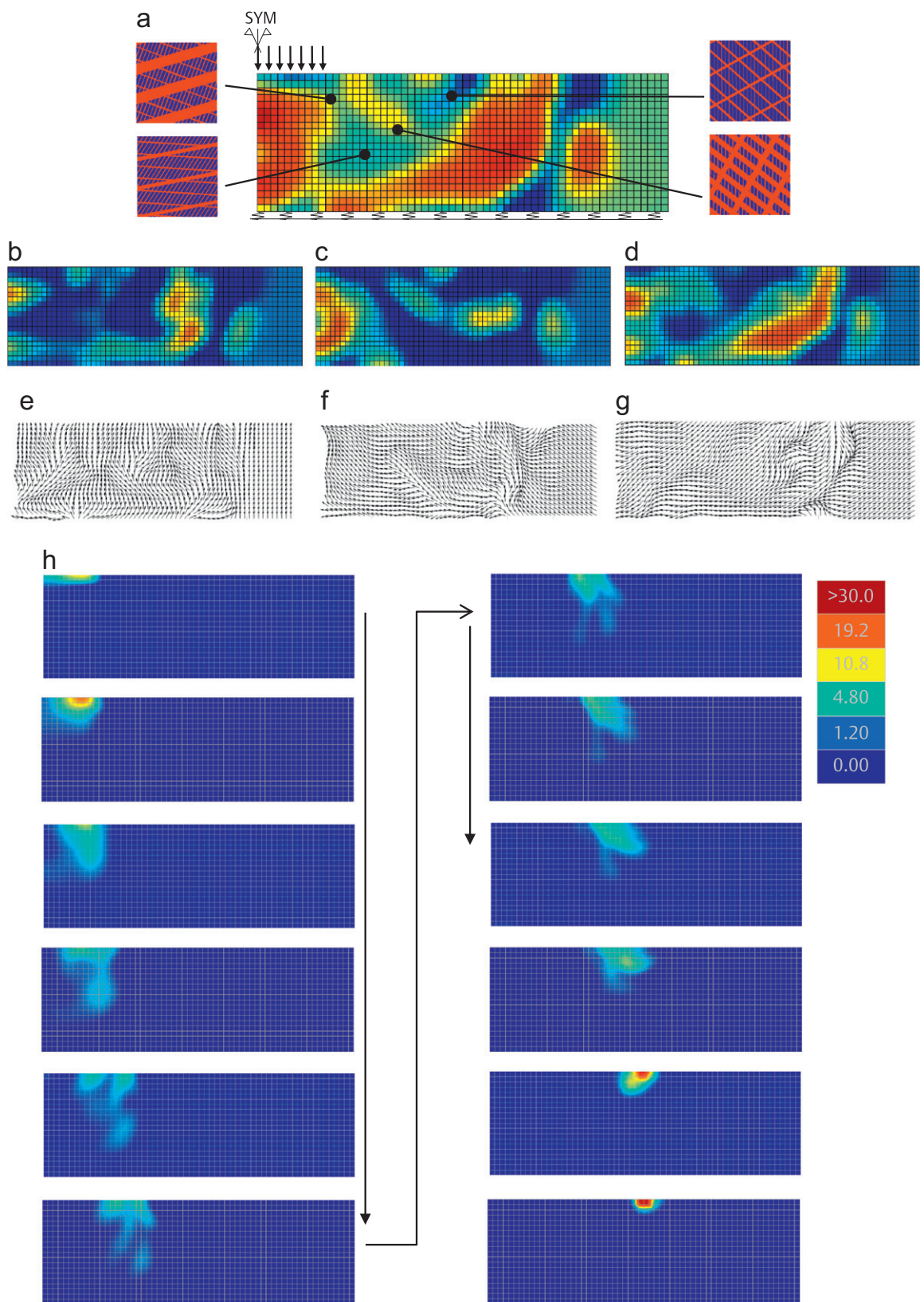


Fig. 15. Energy focusing design: find the rank-3 laminate microstructure to concentrate energy to a top region. (a) Optimal design (overall vol. frac.), (b) Vol. frac., layer 1, (c) Vol. frac., layer 2, (d) Vol. frac., layer 3, (e) Orientation, layer 1, (f) Orientation, layer 2, (g) Orientation, layer 3 and (h) Total energy at times 3.75, 7.5, 10.0, 12.5, 16.25, 20.0, 23.75, 27.5, 30.0, 32.5, 40.0 and 47.5 μ s.

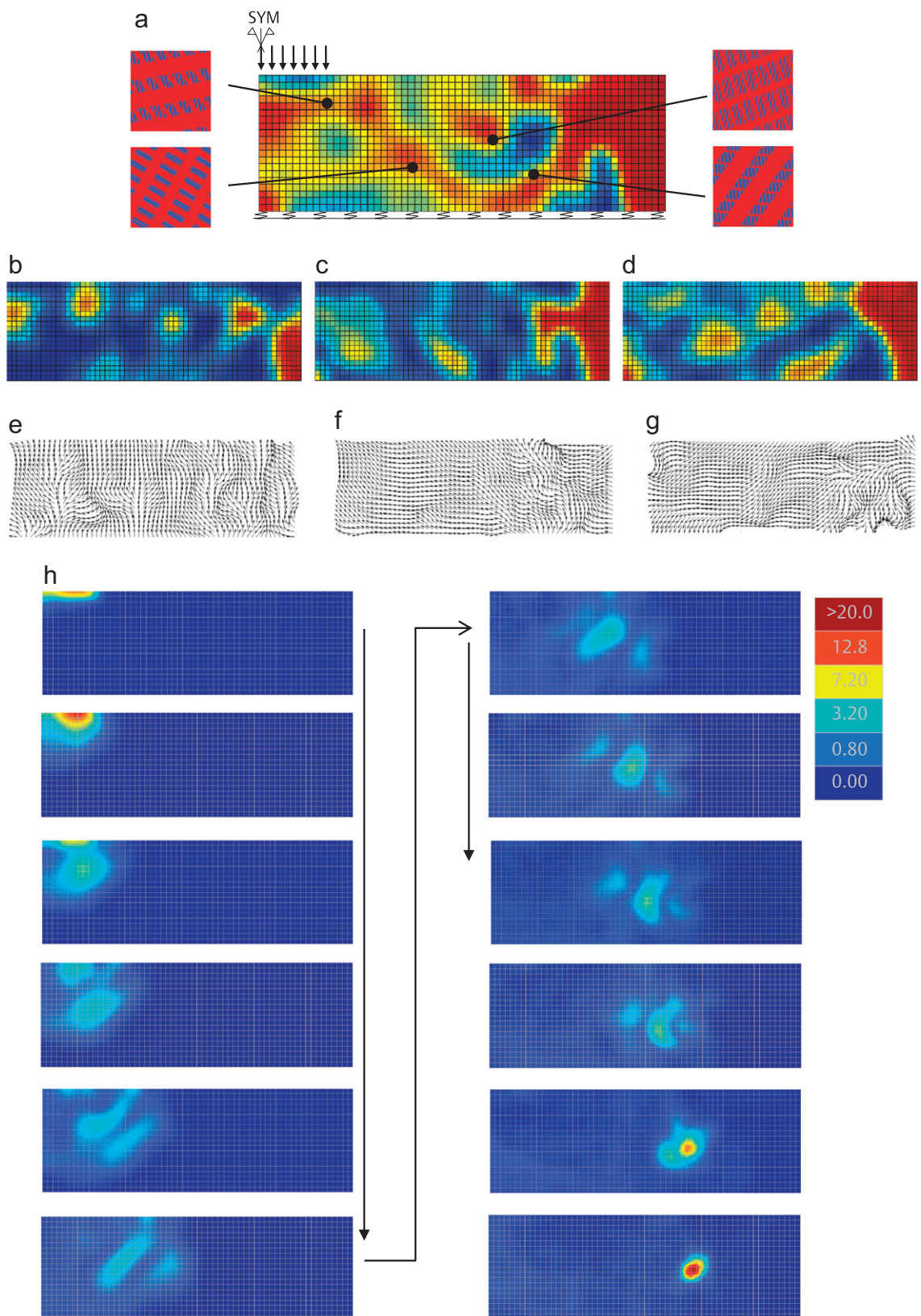


Fig. 16. Energy focusing design: find the rank-3 laminate microstructure to concentrate energy to an interior region. (a) Optimal design (overall vol. frac.), (b) Vol. frac., layer 1, (c) Vol. frac., layer 2, (d) Vol. frac., layer 3, (e) Orientation, layer 1, (f) Orientation, layer 2, (g) Orientation, layer 3 and (h) Total energy at times 3.75, 7.5, 10.0, 12.5, 16.25, 20.0, 23.75, 27.5, 30.0, 32.5, 40.0 and 47.5 μ s.

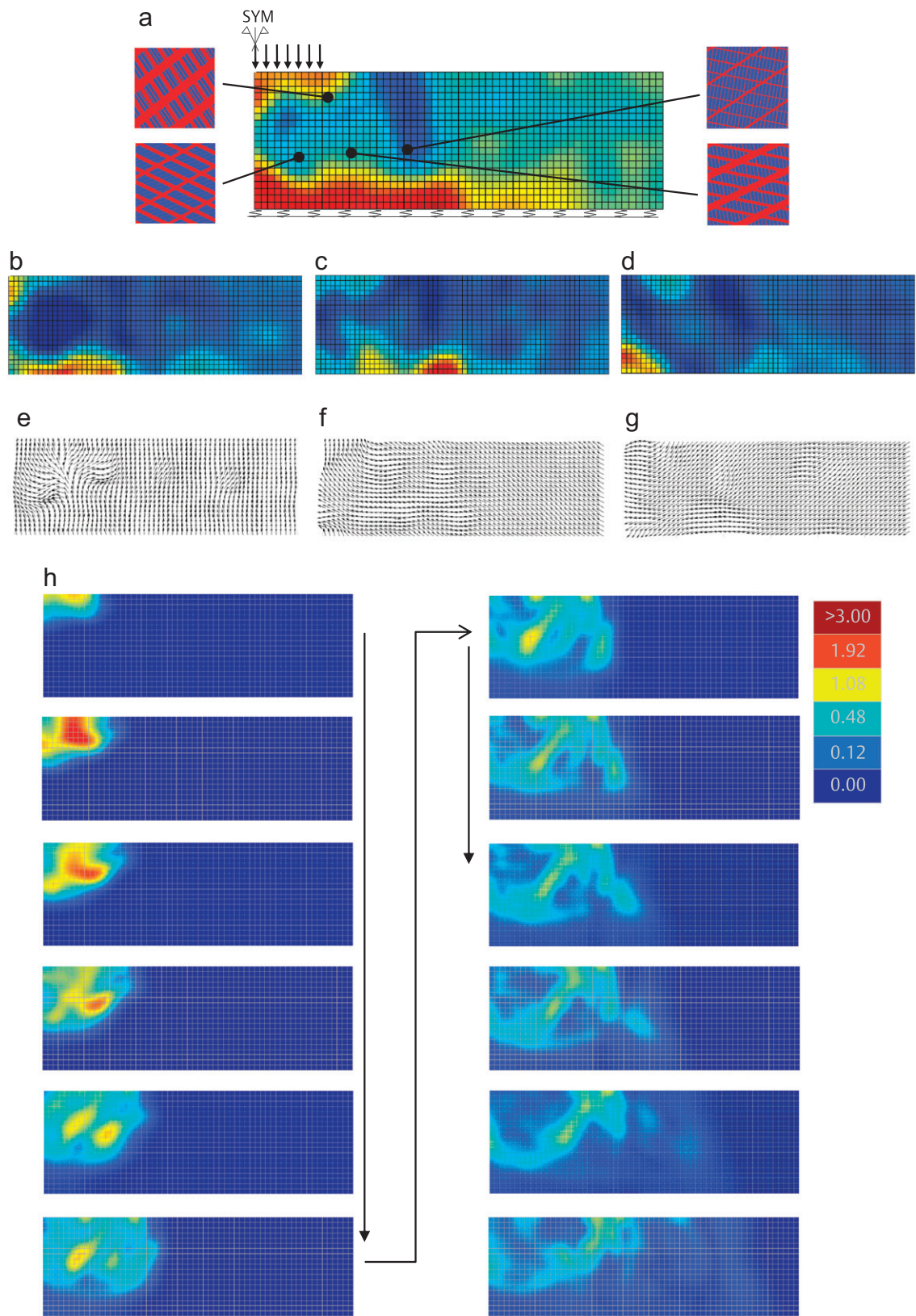


Fig. 17. Energy dispersing design: find the rank-3 microstructure to minimize the maximum total energy at the bottom. (a) Optimal design (overall vol. frac.), (b) Vol. frac., layer 1, (c) Vol. frac., layer 2, (d) Vol. frac., layer 3, (e) Orientation, layer 1, (f) Orientation, layer 2, (g) Orientation, layer 3 and (h) Total energy at times 3.75, 7.5, 10.0, 12.5, 16.25, 20.0, 23.75, 27.5, 30.0, 32.5, 40.0 and 47.5 μ s.

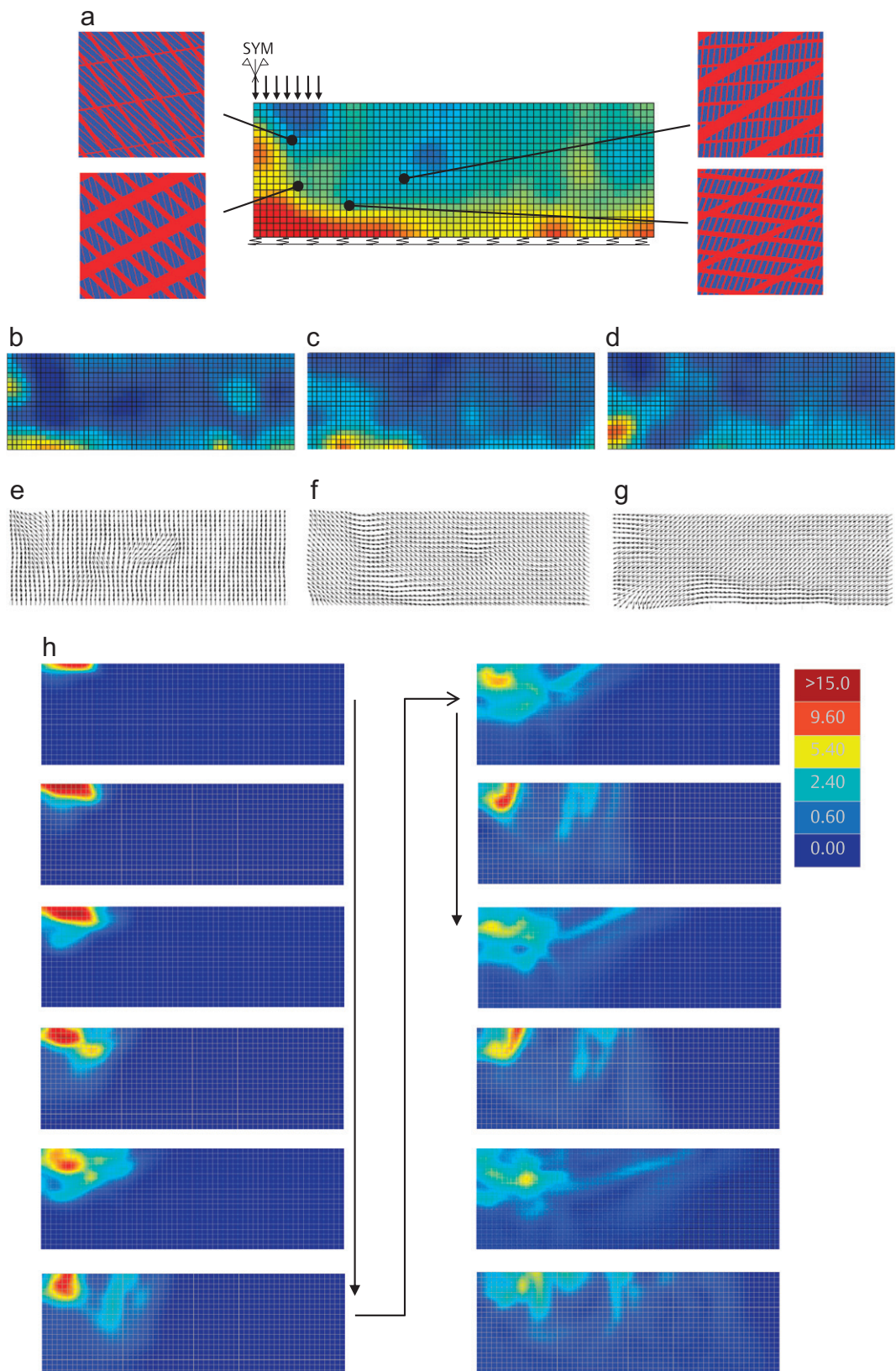


Fig. 18. Energy dispersing design: find the rank-3 microstructure to minimize the normalized maximum total energy at the bottom. (a) Optimal design (overall vol. frac.), (b) Vol. frac., layer 1, (c) Vol. frac., layer 2, (d) Vol. frac., layer 3, (e) Orientation, layer 1, (f) Orientation, layer 2, (g) Orientation, layer 3 and (h) Total energy at times 3.75, 7.5, 10.0, 12.5, 16.25, 20.0, 23.75, 27.5, 30.0, 32.5, 40.0 and 47.5 μ s.

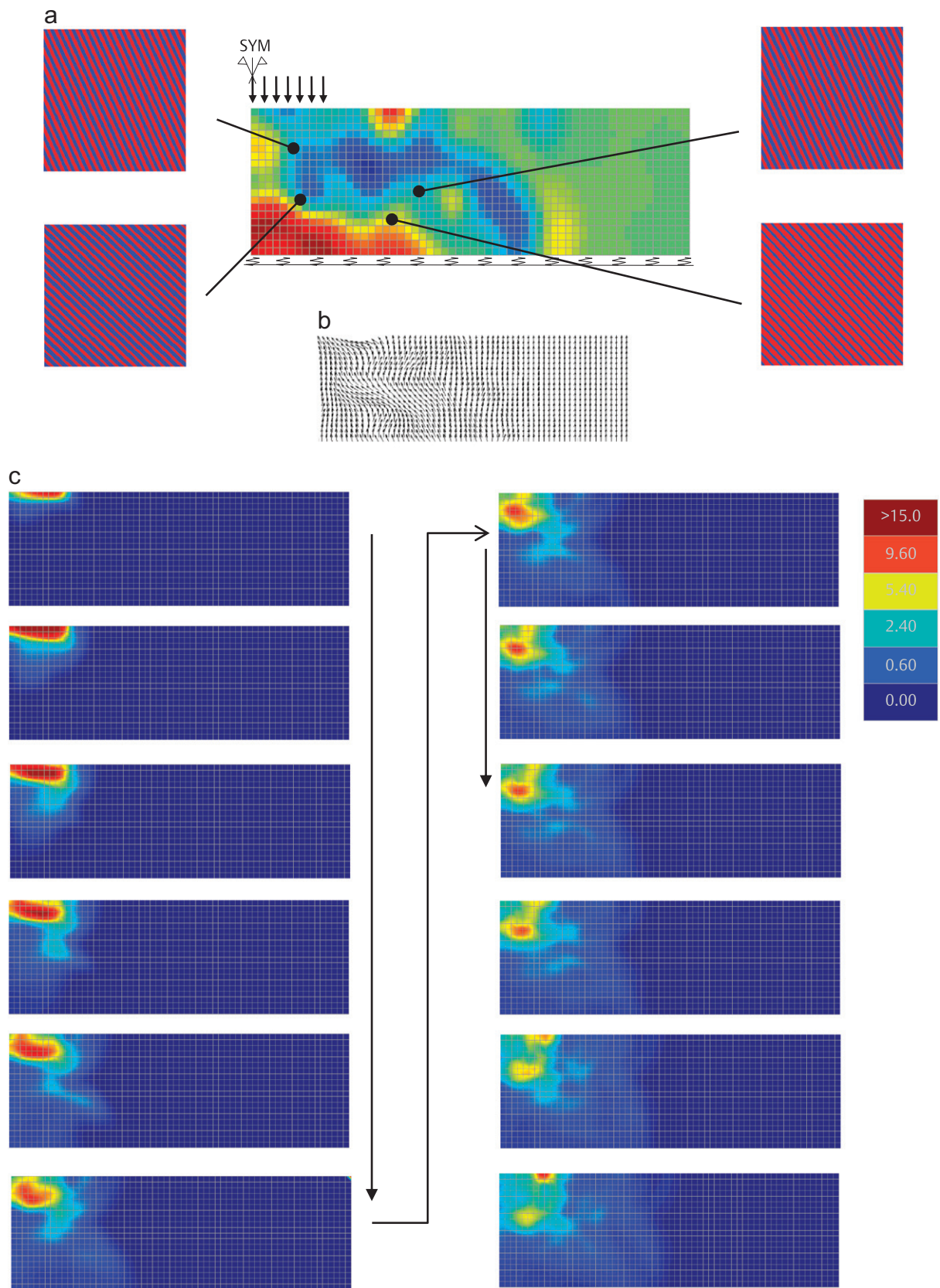


Fig. 19. Energy dispersing design: repeat of example in Fig. 18 using rank-1 laminate. (a) Optimal design (overall vol. frac.), (b) Orientation, layer 1 and (c) Total energy at times 3.75, 7.5, 10.0, 12.5, 16.25, 20.0, 23.75, 27.5, 30.0, 32.5, 40.0 and 47.5 μ s.

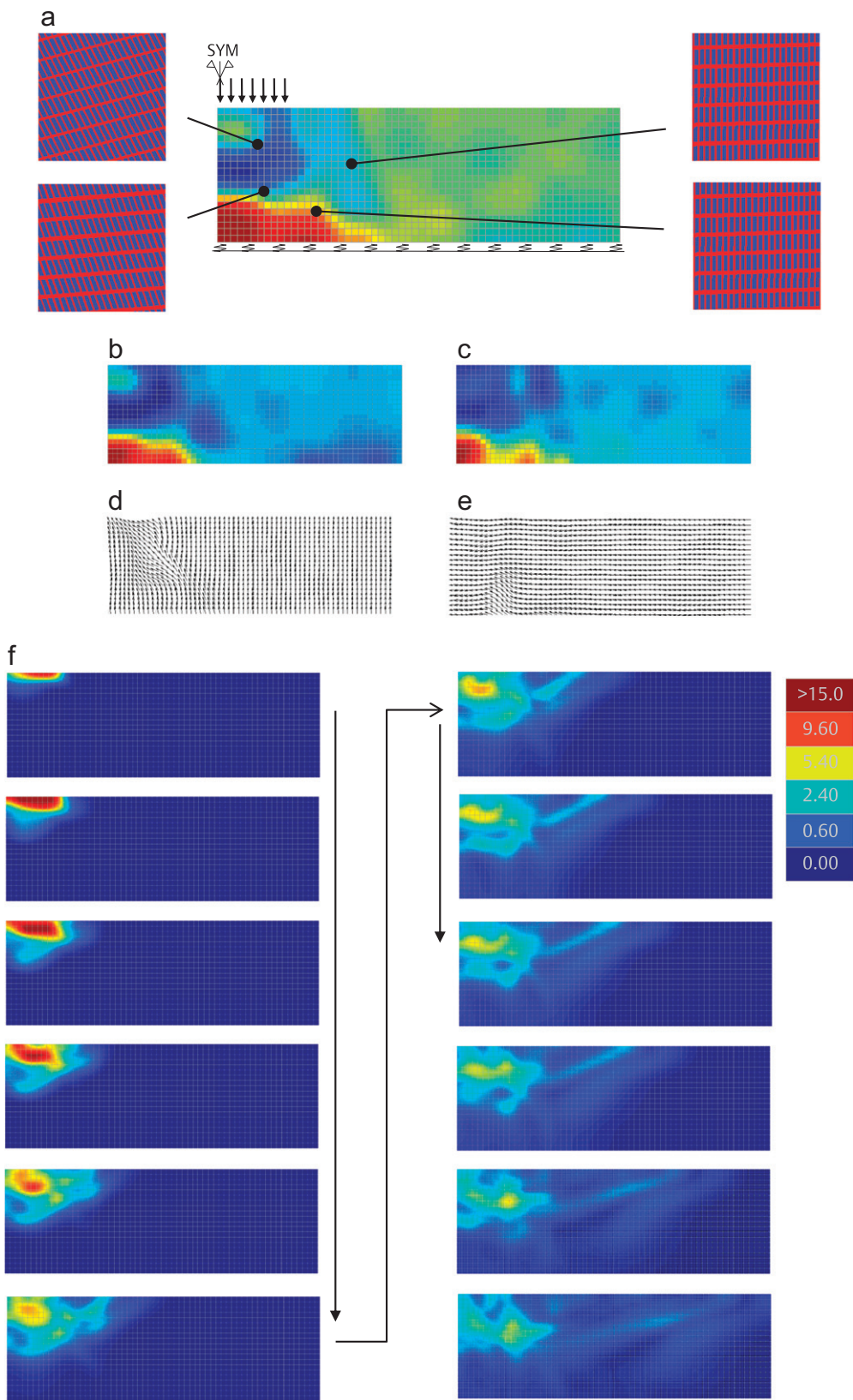


Fig. 20. Energy dispersing design: repeat of example in Fig. 18 using rank-2 laminate. (a) Optimal design (overall vol. frac.), (b) Vol. frac., layer 1, (c) Vol. frac., layer 2, (d) Orientation, layer 1, (e) Orientation, layer 2 and (f) Total energy at times 3.75, 7.5, 10.0, 12.5, 16.25, 20.0, 23.75, 27.5, 30.0, 32.5, 40.0 and 47.5 μ s.

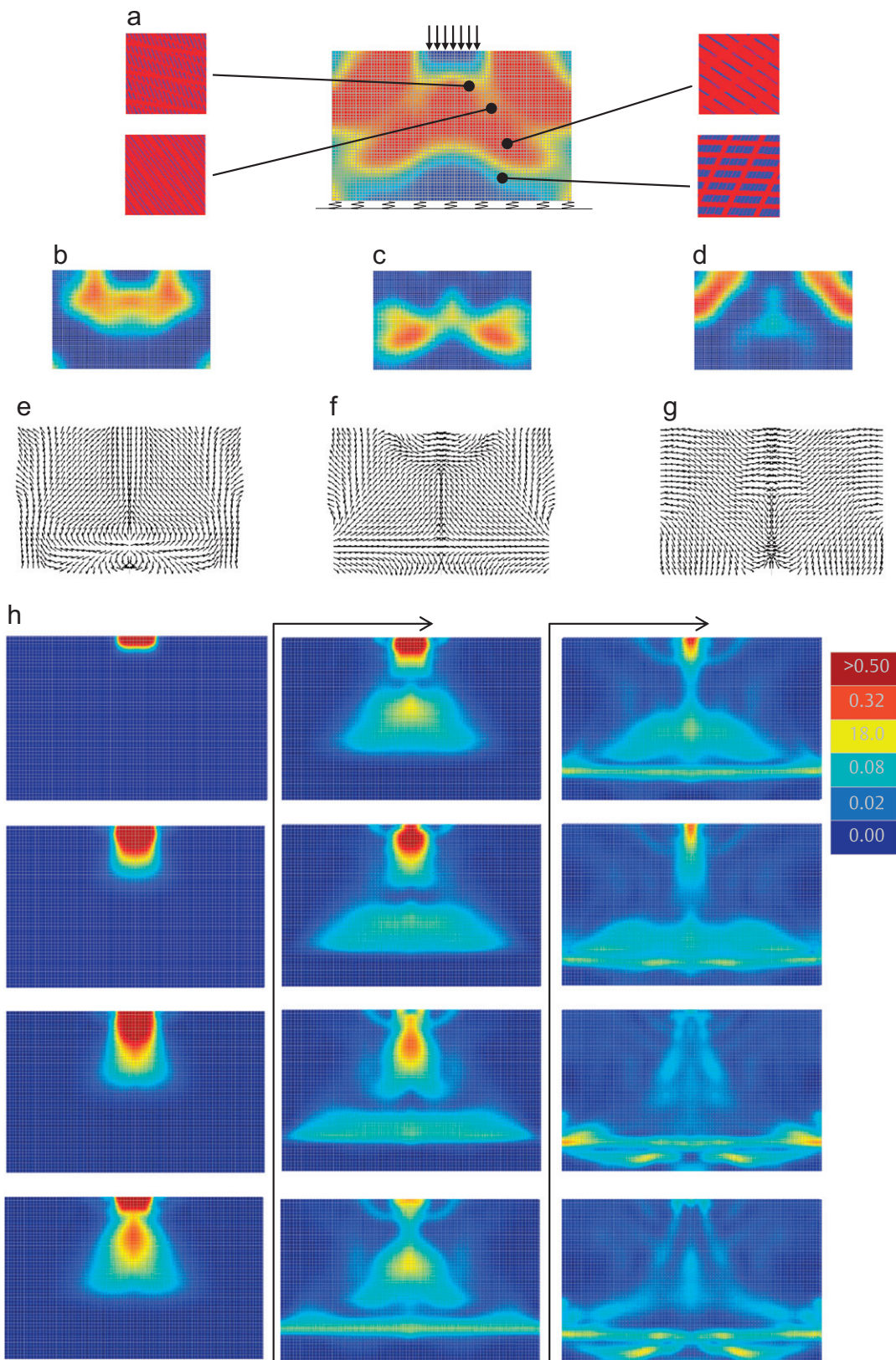


Fig. 21. Energy spreading design: find the rank-3 microstructure to spread the energy evenly near the bottom. (a) Optimal design (overall vol. frac.), (b) Vol. frac., layer 1, (c) Vol. frac., layer 2, (d) Vol. frac., layer 3, (e) Orientation, layer 1, (f) Orientation, layer 2, (g) Orientation, layer 3 and (h) Total energy at times 3.3, 6.6, 8.3, 10.0, 11.7, 13.3, 15.0, 16.7, 18.3, 20.0, 23.3 and 25.0 μ s.

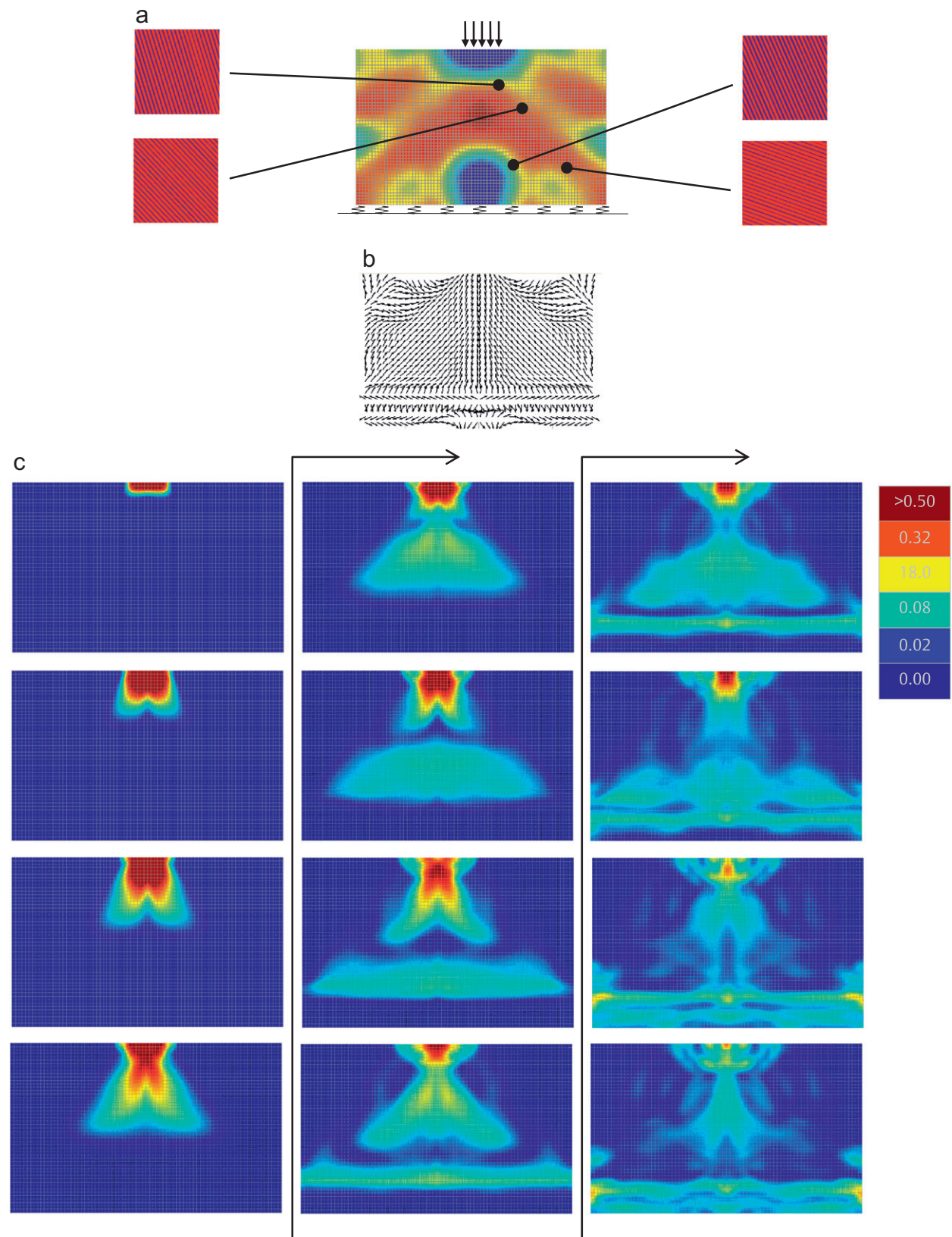


Fig. 22. Energy spreading design: repeat of example in Fig. 21 using rank-1 laminate. (a) Optimal design (overall vol. frac.), (b) Orientation and (c) Total energy at times 3.3, 6.6, 8.3, 10.0, 11.7, 13.3, 15.0, 16.7, 18.3, 20.0, 23.3 and 25.0 μ s.

functions. For example, in Silva et al. (2010) elastostatic structures are optimized to withstand probabilistic loads. This probabilistic consideration is certainly of practical interest, however it is not the subject of this work. Nonetheless, to show the effect of a load variation we perform an analysis on the design illustrated in Fig. 22; however we replace the triangular pulse with an equal area shifted inverted cosine function, i.e. $h/2[1-\cos(2\pi/T)]$ where $h=1$ MPa and $T=10$ μ s. Under this cosine loading the RMS error function value is 0.04368 ($N\text{ mm}$)² as compared to the 0.008226 ($N\text{ mm}$)² value corresponding to the triangular pulse. This small difference is to be expected as the two loadings are similar; more importantly it indicates that our designs appear to be stable with respect to loading variations. Regarding the second robustness issue, we have performed mesh refinement studies (both spatially and temporally) and obtained similar designs, cf. Figs. 5 and 8 vs. Fig. 9. Presumably, if we used alternate element formulations or time stepping schemes we would produce different designs; however we expect these differences to be negligible. For example, we have obtained similar designs using both energy conserving explicit and energy conserving implicit time integration schemes.

6. Conclusions

We have demonstrated that optimization (more specifically topology optimization) can be used to effectively design material microstructures for tailored energy propagation. This capability may lead to exciting applications although fabrication and experimental verification must of course be performed. We note that our design optimization, as an initial study, is based on “low frequency” homogenization in the linear regime, and for a specific sequentially ranked laminate microstructure. Extending to other behavior regimes and microstructures are subjects for future investigations.

Acknowledgments

We thank Prof. G. Allaire at the CMAP, Ecole Polytechnique and the reviewers for their insightful comments. This work was funded by the US Army Research Office under MURI Grant #W911NF-09-1-0436 (Dr. David Stepp program monitor).

Appendix A. Supporting information

Supplementary data associated with this article can be found in the online version at doi:[10.1016/j.jmps.2011.09.002](https://doi.org/10.1016/j.jmps.2011.09.002).

References

- Allaire, G., 2002. Shape Optimization by the Homogenization Method. Springer-Verlag, New York.
- Allaire, G., Jouve, F., Maillot, H., 2004. Topology optimization for minimum stress design with the homogenization method. *Struct. Multidisciplinary Optim.* 28 (2–3), 87–98.
- Amirkhizia, A., Tehrani, A., Nemat-Nasser, S., 2010. Stress-wave energy management through material anisotropy. *Wave Motion* 47 (8).
- Bendsøe, M., 1989. Optimal shape design as a material distribution problem. *Struct. Multidisciplinary Optim.* 1 (4), 193–202.
- Bendsøe, M., Kikuchi, N., 1988. Generating optimal topologies in structural design using a homogenization method. *Comput. Methods Appl. Mech. Eng.* 71 (2), 197–224.
- Bendsøe, M., Sigmund, O., 2003. Topology Optimization: Theory, Methods and Applications. Springer-Verlag, Berlin.
- Bensoussan, A., Lions, J., Papanicolaou, G., 1978. Asymptotic Analysis for Periodic Structures. North-Holland Publishing Company, Amsterdam.
- Brahim-Otsmane, S., Francfort, G., Murat, F., 1992. Correctors for the homogenization of the wave and heat equations. *J. Math. Pures Appl.* 71 (3), 197–231.
- Cheng, K.-T., Olhoff, N., 1982. Regularized formulation for optimal design of axisymmetric plates. *Int. J. Solids Struct.* 18 (2), 153–169.
- Cherkaev, A., 2000. Variational Methods for Structural Optimization. Springer-Verlag, New York.
- Cook, R., Malkus, D., Plesha, M., Witt, R., 2002. Concepts and Applications of Finite Element Analysis. John Wiley & Sons, New York.
- Cox, S., Dobson, D., 2000. Band structure optimization of two-dimensional photonic crystals in h-polarization. *J. Comput. Phys.* 158 (2), 214–224.
- Dahl, J., Jensen, J., Sigmund, O., 2008. Topology optimization for transient wave propagation problems in one dimension. *Struct. Multidisciplinary Optim.* 36, 585–595.
- Díaz, A., Sigmund, O., 1995. Checkerboard patterns in layout optimization. *Struct. Multidisciplinary Optim.* 10 (1), 40–45.
- Díaz, R., Lipton, R., 1997. Optimal material layout for 3d elastic structures. *Struct. Multidisciplinary Optim.* 13 (1), 60–64.
- Frei, W., Tortorelli, D., Johnson, H., 2005. Topology optimization of a photonic crystal waveguide termination to maximize directional emission. *Appl. Phys. Lett.* 86 (11), 111114.
- Hashin, J., Shtrikman, S., 1963. A variational approach of the theory of elastic behavior of multiphase materials. *J. Mech. Phys. Solids* 11 (2), 127–140.
- Haug, E., Arora, S., 1978. Design sensitivity analysis of elastic mechanical systems. *Comput. Methods Appl. Mech. Eng.* 15 (1), 35–62.
- Haug, E., Choi, K., Komkov, V., 1986. Design Sensitivity Analysis of Structural Systems. Academic Press.
- Hollister, S., Kikuchi, N., 1992. A comparison of homogenization and standard mechanics analyses for periodic porous composites. *Comput. Mech.* 10 (2), 73–95.
- Hulbert, G.M., Chung, J., 1996. Explicit time integration algorithms for structural dynamics with optimal numerical dissipation. *Comput. Methods Appl. Mech. Eng.* 137 (2), 175–188.
- Jacobsen, B., Olhoff, N., Rønholz, E., 1998. Generalized shape optimization of three-dimensional structures using materials with optimum microstructures. *Mech. Mater.* 28 (1–4), 207–225.
- Jensen, J., Sigmund, O., 2005. Topology optimization of photonic crystal structures: a high-bandwidth low-loss t-junction waveguide. *J. Opt. Soc. Am. B* 22 (6), 1191–1198.
- Jog, C.S., Haber, R., 1996. Stability of finite element models for distributed parameter optimization and topology design. *Comput. Methods Appl. Mech. Eng.* 130 (3–4), 203–226.
- Kohn, R., Strang, G., 1986. Optimal-design and relaxation of variational-problems. *Commun. Pure Appl. Math.* 22 (1–3), 113–137 139–182; 353–377.

- Larsen, A., Laksafoess, B., Jensen, J., Sigmund, O., 2009. Topological material layout in plates for vibration suppression and wave propagation control. *Struct. Multidisciplinary Optim.* 37 (6), 585–594.
- Lurie, K., Cherkaev, A., 1986. Effective characteristics of composite materials and the optimal design of structural elements. *Usp. Mekh.* 9 (2), 3–81.
- Michaleris, P., Tortorelli, D., Vidal, C., 1994. Tangent operators and design sensitivity formulations for transient nonlinear coupled problems with applications to elastoplasticity. *Int. J. Numer. Methods Eng.* 37 (14), 2471–2499.
- Michell, A., 1904. The limits of economy of material in frame structures. *Philos. Mag.* 8, 589–597.
- Min, S., Kikuchi, N., Park, Y., Kim, S., Chang, S., 1999. Optimal topology design of structures under dynamic loads. *Struct. Multidisciplinary Optim.* 17 (2–3), 1488–1615.
- Munch, A., Pedregal, P., Periago, F., 2006. Optimal design of the damping set for the stabilization of the wave equation. *J. Differential Equations* 231 (1), 331–358.
- Murat, F., Tartar, L., 1985. Calcul des variations et homogénéisation. *Les Méthodes de l'Homogénéisation Théorie et Applications en Physique*, pp. 319–369.
- Murat, F., Tartar, L., 1997. H-convergence. *Topics in the Mathematical Modelling of Composite Materials. Progress in Partial Differential Equations and their Applications*, vol. 31., Birkhäuser Boston Inc., Boston, pp. 21–44.
- Nomura, T., Nishiwaki, S., Sato, K., K, H., 2009. Topology optimization for the design of periodic microstructures composed of electromagnetic materials. *Finite Elem. Anal. Des.* 45 (3), 210–226.
- Norris, A., Wickham, G., 2001. Elastic waves in inhomogeneously oriented anisotropic materials. *Wave Motion* 33 (1), 97–107.
- Olhoff, N., Rønholt, E., Scheel, J., 1998. Topology optimization of three-dimensional structures using optimal microstructures. *Struct. Multidisciplinary Optim.* 16 (1), 1–18.
- Rodrigues, C., Guedes, J., Bendsøe, M., 2002. Hierarchical optimization of material and structures. *Struct. Multidisciplinary Optim.* 24 (1), 1–10.
- Rodrigues, C., Jacobs, C., Guedes, J., Bendsøe, M., 1998. Global and local material optimization models applied to anisotropic bone adaptation. In: *IUTAM Symposium on Synthesis in Bio Solid Mechanics*.
- Rodrigues, H., Fernandes, P., 1995. A material based model for topology optimization of thermoelastic structures. *Int. J. Numer. Methods Eng.* 38 (12), 1951–1965.
- Rozvany, G., 1998. Exact analytical solutions for some popular benchmark problems in topology optimization. *Struct. Multidisciplinary Optim.* 15 (1), 42–48.
- Sigmund, O., Jensen, J., 2003. Systematic design of phononic band-gap materials and structures by topology optimization. *Philos. Trans. R. Soc. London Ser. A Math. Phys. Eng. Sci.* 361 (1806), 1001–1019.
- Sigmund, O., Petersson, J., 1998. Numerical instabilities in topology optimization: a survey on procedures dealing with checkerboards, mesh-dependencies and local minima. *Struct. Multidisciplinary Optim.* 16 (1), 69–75.
- Silva, M., Tortorelli, D., Norato, J., Ha, C., Bae, H., 2010. Component and system reliability-based topology optimization using a single-loop method. *Struct. Multidisciplinary Optim.* 41 (1), 87–106.
- Svanberg, K., 1987. The method of moving asymptotes—a new method for structural optimization. *Int. J. Numer. Methods Eng.* 24 (2), 359–373.
- Tortorelli, D., Lu, S., Haber, R., 1990. Design sensitivity analysis for elastodynamic systems. *Mech. Struct. Mach.* 18 (1), 77–1062.
- Turteltaub, S., 2005. Optimal non-homogeneous composites for dynamic loading. *Struct. Multidisciplinary Optim.* 30 (2), 101–112.
- Zhou, M., Rozvany, G., 1991. The COC algorithm, Part ii: topological, geometrical and generalized shape optimization. *Comput. Methods Appl. Mech. Eng.* 89 (1–3), 209–336.